

Resonances in Extrasolar Planetary Systems

Hanno Rein

January 13, 2009

Abstract

Ever since we began to observe the sky, mankind was fascinated by the movement of wandering stars (planets). For a long time the observations have been confined to our own solar system, but nowadays we have evidence of more than 330 wandering stars orbiting many different suns. Thanks to new observational methods becoming available right now, the subject is evolving rapidly and is one of the most exciting areas in astronomy: after all, we are searching for a second Earth.

In part I of this essay I give an introduction to the current status of exo-planet observations and recapitulate important background material on planet formation, celestial mechanics and numerical techniques used later on.

In part II, I focus on multiple planets that are in resonance. A resonance is a special configuration of the orbital parameters such that the period of one planet is an integer multiple of the other planet's period. This is an important characteristic of the observed exoplanets which allows us to study the evolution of the planetary system in great detail. The discs in which planets form are thought to be turbulent and therefore planets feel random forces. This may eventually break the resonance. The fact that we observe resonant systems today tells us a lot about the properties of the turbulence during the time when the planets were formed.

Units and symbols as well as longer calculations involving dissipative forces on planets and the calculation of orbital elements are listed in the appendix.



St John's College
Cambridge

University of Cambridge
Department of Applied Mathematics
and Theoretical Physics



Declaration

The work contained in this essay was carried out by myself and in collaboration with my supervisor Professor John C. B. Papaloizou.

Part I constitutes an introduction to planet formation and a review of relevant background material. It does not contain original research and the experienced reader may skip this part. The second part is based on a paper which is currently being written (Rein & Papaloizou 2009, in preparation) and contains original research. The analytic part was done in collaboration with my supervisor. The source code used for simulations in part II was developed and run by myself. All figures in this essay were created by myself. The appendix does not contain original research. References are given therein.

Hanno Rein

John C. B. Papaloizou

Contents

I	Introduction	6
1	Planet Formation	7
1.1	History of Extrasolar Planets	7
1.2	Observational Techniques	8
1.3	Observed Objects	9
1.4	Magnetorotational Instability	10
2	Methods and Conventions	11
2.1	N-Body Simulations	11
2.2	Numerical Integrators	12
2.3	Celestial Mechanics	12
2.4	Elliptic Orbit	13
II	Turbulence and Mean Motion Resonances	16
3	Overview	17
4	Basic Equations	19
4.1	Additional Forcing of a Single Planet	19
4.2	Multiple Planets	20
4.2.1	Equations of Motion	21
4.2.2	Modes of Libration	22
4.2.3	Fast Mode	22
4.2.4	Slow Mode	23
4.2.5	Librations with External Forcing	23
4.3	Stochastic Forces	24
4.3.1	Stochastic Forcing of an Isolated Planet	25
4.3.2	Stochastic Variation of the Resonant Angles in the Two Planet Case . . .	26
4.3.3	Growth of Libration Amplitudes	27
5	Numerical Simulations	28
5.1	Stochastic Forces	28
5.2	Numerical Implementation	30
5.3	Stochastic Forces Acting on a Single Planet	31
5.4	Illustration of the Modes of Libration in a Two Planet System	31

6	Two Planets with Stochastic Forcing	34
6.1	Disruption of a Resonance in Stages	34
6.1.1	Attainment of Circulation of the Angle Between the Apsidal Lines	36
6.1.2	Attainment of Circulation of the Fast Angle	36
6.1.3	A Numerical Illustration	36
6.2	Dependence on the Diffusion Coefficient	38
7	Formation of HD128311	41
7.1	Migration Forces	42
7.2	Adiabatic Invariance and the Stabilization of Librations through Migration	42
7.3	Model 1	45
7.4	Model 2	45
7.5	Model 3	45
8	Discussion	47
9	Acknowledgements	49
III	Appendix	50
A	Units and Symbols	51
B	Dissipative Forces on Planets	53
C	Calculating Orbital Elements	55

Part I

Introduction

Chapter 1

Planet Formation

1.1 History of Extrasolar Planets

In 1713, Isaac Newton wrote in an essay attached to the third edition of his famous *Principia Mathematica*

And if the fixed Stars are the Centers of other like systems, these, being form'd by like wise counsel, must be all subject to the dominion of One, [...].¹

In other words, he expected to see planets around other stars. Over 275 years later, astronomers discovered the first planet beyond our own solar system, a so called exoplanet. Since then the number of known planets has increased rapidly. To date, 334 exoplanets have been discovered (for the latest numbers, see <http://exoplanet.eu>).

There are at least 25 multi-planet systems with two or more planets among the discovered extrasolar planets. They are of particular interest because they give new insights into the planet formation process.

Planets are believed to form in protostellar discs as a natural by-product of star formation. These discs are made of the same material as the star itself, gas and dust. Current theories give two possible explanations of the formation of giant planets inside the disc:

The Core Accretion Model. Solid components of the disc stick together, forming bigger and bigger objects until a core of about 15 Earth masses is formed (?). The protoplanet then starts to accrete gas and forms a gas giant. In the past, one problem in this theory arose because the timescale needed for the process was thought to be longer than the disc lifetime. However, detailed studies involving turbulent discs and a more realistic gas/dust feedback show that the timescale might not be so large after all.

Gravitational Fragmentation. In this model, the gas planets form directly as a result of gravitational instability within the disc (?); no solid core is needed. However, the planet can still form a core by accreting dust particles later on.

For the gravitational instability to occur, it is necessary to have a Toomre Q parameter of less than unity (?). This parameter was first introduced in a study of galaxy formation and it is not clear if the physical conditions in a protoplanetary disc are compatible with this constraint.

¹General Scholium, translated by Motte (1729)

Both models favour planet formation at much larger radii compared to the observed positions of planets. However, in any model the disc interacts with the newly formed protoplanet. Density waves are excited in the disc both interior and exterior to the planet. The waves carry angular momentum and produce a torque on the planet that can lead to planetary migration (?). The direction of migration depends on the exact disc model. In most cases, the outer torque is bigger than the inner one. Thus the planet migrates inwards (?). This effect is called type I migration.

If the planet is massive enough, it can open a gap in the disc. For most disc models about a Jupiter mass is needed to clear a gap. The process is similar to the gaps opening in Saturn's rings with moons orbiting inside. The planet still interacts with the disc and migrates (type II migration).

Usually one assumes that the Navier-Stokes equations are valid within the disc and that there is an anomalous high viscosity. This is needed to reproduce the observed accretion rates. It is not a molecular viscosity but an effective viscosity that originates from turbulence. More details on this are given in section 1.4.

If there are two (or more) planets in the disc the migration rates might differ. The resulting differential migration changes the ratio of orbital periods T_i and the ratio of semi major axes a_i . The ratios are related by Kepler's Third Law

$$\frac{T_1}{T_2} = \left(\frac{a_1}{a_2}\right)^{\frac{3}{2}} \quad (\text{Kepler's Third Law}). \quad (1.1)$$

The planets can become locked into a mean motion resonance (MMR) if this ratio gets close to a rational number; e.g. $\frac{1}{2}, \frac{1}{3}, \frac{2}{3}$. Most resonances are stable and planets stay in resonance over a very long period of time, migrating together. The process of resonance capturing might explain the observed resonant multi-planet systems like GJ876 or 55 Cancri (??).

So far, only preliminary work has been done on studying the effect of the MRI on resonance capturing (??). If the turbulence is active long enough, it will eventually kick the planets out of resonance. However, the timescale needed for destroying the resonance is not well constrained. We present new results on this issue in the next part of this essay.

1.2 Observational Techniques

There are various different techniques available to detect exoplanets. Each of them has advantages and disadvantages. We summarise them in this section because the sparse information we get from those detections determines the predictability of our theoretical work.

Radial Velocity Measurements Most planets have been discovered by the radial velocity (RV) method. Not only the planet is orbiting the centre of mass in the system, but also the star. The radial part of this movement can be measured as a Doppler shift in one of the host star's spectral lines with high precision spectrometry. Once we determined the mass of the star by stellar evolution models, we can fit different orbital configurations trying to reproduce the observed light curve.

This method biases the detection of massive planets on short orbits (Hot Jupiters, see below) as the gravitational influence by the planet on the star is bigger in those cases.

Only a limited number of parameters can be obtained by the RV method. Because there is a degeneracy in the inclination i (it is not possible to measure the non-radial part of the

velocity), we can only get an upper limit on the mass of the planet: $m \geq m \cdot \sin i$. Other orbital parameters that can be obtained are the semi major axis a and the eccentricity e .

Transit Light Curves It is possible to observe transits of planets in front of their host stars. This is not only true in the solar system with Mercury and Venus, but also in exoplanetary systems.

The transit method is capable of measuring the density ρ of exoplanets and thus adds an important parameter to the list of observed quantities compared to the radial velocity method. It is even possible to do spectroscopy on the atmosphere of the planet during the transit or the secondary transit (this is when the planet goes behind the star) and create a temperature map of the exoplanet (see eg. ?). Unfortunately transits are rare because the host star, the exoplanet and Earth have to be aligned in one line for a transit to occur. However, present and future dedicated ground and space based missions promise to detect a large number of planets in the near future.

Gravitational Microlensing If a massive object like a star is aligned in one line with the earth and a bright object in the background (eg. another star), the light from the background object bends and can be detected by an increase in luminosity from earth. This is called gravitational microlensing. A planet in an orbit around the star can disturb the light curve and theoretical models can determine the planet's mass and orbital parameters. This event happens only once per star, so good timing and a global collaboration is needed to perform a precise measurement of the light curve. The first exoplanet was discovered by gravitational microlensing in 2004 by ?

Direct Imaging In 2004 ? reported the first detection of a giant planet candidate by direct imaging. The object is very massive and thus it is not clear whether it can be called planet or not (see below). Recently, two more groups reported the detection of multiple planets by direct imaging (??).

Pulsar Timing The first exoplanet was discovered by the pulsar timing method (?). By measuring slight variations in the regular timings from a pulsar, it is possible to detect the perturbations created by a planetary companion. This is sensitive down to very small mass planets. However, pulsars are rare compared to normal stars within our galaxy. That is why we do not expect to discover many planets by this method.

1.3 Observed Objects

A lot of objects detected so far are called 'Hot Jupiters'. Their size and mass is comparable to Jupiter but their orbits are very close (≈ 0.05 AU) to their host star with periods of the order of a few days. Thus, the expected surface temperatures are very high. Most detection methods described above bias detections in favour of these objects. However, the existence of hot Jupiters still results in difficulties for planet formation theories (Note that there are no Hot Jupiters in our own solar system). The so called snow line, where the temperature is low enough such that water ice can exist, lies at much large radii. Beyond the snow line planets are formed easier. As described above, planetary migration is one solution to this problem.

Other observed objects are very heavy and are more likely to be brown dwarfs and stars rather than planets. It is not clear where the borderline between stars and planets lies. However, the International Astronomical Union (IAU) defines an extrasolar planet as follows:

Objects with true masses below the limiting mass for thermonuclear fusion of deuterium (currently calculated to be 13 Jupiter masses for objects of solar metallicity) that orbit stars or stellar remnants are "planets" (no matter how they formed). The minimum mass/size required for an extrasolar object to be considered a planet should be the same as that used in our Solar System. (?)

The Holy Grail for exoplanet hunters is another earth-like planet that orbits the host star within the habitable zone. Such a planet might be capable of sustaining life. At the present day, the planet that is closest to one earth mass is PSR B1257+1 C which orbits a pulsar and has a mass of approximately 3.9 earth masses.

1.4 Magnetorotational Instability

Accretion discs have been observed for a long time. The angular momentum of the accreting material has to be transported outwards. Therefore, it is possible to determine the angular momentum flux in the discs by measuring the accretion rate. The strength of this mechanism can be parametrised by a dimensionless viscosity $\alpha = \nu_t / (c_s H)$ (?) with typical values of $10^{-3} - 10^{-2}$. The viscosity needed for the observed angular momentum transport is most likely generated by the magnetorotational instability, MRI (see ?, ?). The MRI can occur in ionised and weakly magnetised discs. A protoplanetary disc is thought to have all the ingredients for the MRI to operate, at least in the top and bottom layers, where cosmic rays increase the ionisation fraction.

The MRI produces density waves of the order of $\delta\rho/\rho \approx 10\%$ (?). These waves interact gravitationally with planets embedded in the disc and can alter their orbital parameters. The force on the planets is stochastic and results to a first approximation in a random walk in the orbital parameters. We derive an analytic model of this effect and show results of numerical simulations in the next part of this essay.

Before we move on, we shortly summarize the numerical techniques and conventions used in the next chapter.

Chapter 2

Methods and Conventions

2.1 N-Body Simulations

In an N-body simulation all objects (e.g. stars, planets) are treated as point masses interacting only gravitationally with each other. To model the planet-disc interaction, one can add dissipative and stochastic forces. Thus, the total force acting on an object i is a sum of the following terms

$$\vec{F}_i = \vec{F}_i^{\text{gravity}} + \vec{F}_i^{\text{indirect}} + \vec{F}_i^{\text{a-damping}} + \vec{F}_i^{\text{e-damping}} + \vec{F}_i^{\text{stochastic}}. \quad (2.1)$$

The first term is due to the gravitational interaction. In units where $G = 1$ we have

$$\vec{F}_i^{\text{gravity}} = \sum_{j \neq i} m_i m_j \frac{r_j - r_i}{|r_j - r_i|^3}, \quad (2.2)$$

where we sum over all particles in the system, except the i -th particle. In the heliocentric coordinate system that we are using the star is located at a fixed position at $\vec{r} = 0$. That brings about an additional indirect term as we are in an accelerated frame,

$$\vec{F}_i^{\text{indirect}} = - \sum_j m_i m_j \frac{r_j}{|r_j|^3}. \quad (2.3)$$

The next two terms are due to the planet-disc interaction. In a first approximation the interaction damps the semi-major axis a and the eccentricity e on time scales τ_a and τ_e , respectively. The exact terms depend on the orbital parameters of the planet and are given in the appendix. It is common practice to define the ratio between the timescales $|\tau_a| \equiv K \cdot \tau_e$. To obtain those timescales, we have to compare the N-body simulations with full hydrodynamical simulations. Once that is done, the simplified model is much faster than a hydrodynamical simulation and thus can be integrated over a longer time span. This is essential because resonance capturing and migration act on timescales ≈ 20000 years and we might even want to integrate over millions of years. The last term simulates stochastic forces.

In order to solve the equations of motion, we developed a new N-body code, written in C++, that is highly modular and easily extendable. It incorporates different modules for turbulence, migration, data output and timestepping. We describe shortly the numerical integrators in the following section. This code was used for all computations in part II of this essay.

2.2 Numerical Integrators

Newton's second law together with the force (2.1) forms a system of ordinary differential equations. We can use various integrators to solve it. The choice of integrator depends on the problem. Integrators with a fixed timestep require some insight into the physical problem to determine the timestep. However, by choosing a sufficiently small timestep, they can for example be used to test other integrators. More complex methods as the Burlirsch-Stoer method are faster. These are able to choose a timestep on their own if one defines a required precision. Another important property is usually the exact (to machine accuracy) conservation of energy. However, as the systems we are considering have an explicit damping term, this is not crucial for our simulations. We implemented the following algorithms:

Runge-Kutta Method (RK4) The classical fourth order Runge-Kutta method is a widely-used standard integrator. It is an explicit method that needs four function evaluations per timestep.

Runge-Kutta-Fehlberg Method (RKF45) The main disadvantage of the RK4 method is the fixed timestep. We have to set a specific value at the beginning of the computation that is not refined later on. The Runge-Kutta-Fehlberg method (?) is a fifth order explicit method with an embedded fourth order method. We can use the two different results to estimate the numerical error and an optimal time step. We repeat the step with a smaller timestep if the error is larger than a specified limit *eps*.

Midpoint Method The midpoint method belongs to the class of second order Runge-Kutta methods. It was implemented because the Bulirsch-Stoer method uses it to calculate the sub-steps. Due to low order it is not efficient to use it on its own.

Bulirsch-Stoer Method (BS) This method (??) is based on a stepwise extrapolation. For each timestep we calculate the result many times with different sub-timesteps Δt_i using the modified midpoint method. We then perform an extrapolation to a perfect sub-step in the limit where $\Delta t \rightarrow 0$. This allows us to use very large timesteps. We can also use the extrapolation to estimate the error and thus make the method adaptive.

2.3 Celestial Mechanics

Our modern approach to celestial mechanics is based on the universal law of gravity. However, Ptolemy, Johannes Kepler and many others were able to calculate the relative motion of planets on the sky long before Isaac Newton discovered the fundamental physical laws of classical mechanics and gravity.

The early models used geometric constructions. Those were not based on any physical law, but relied solely on past observations. It is easy to see that the planets move on quasi-periodic paths. By increasing the number of different frequencies involved, one can obtain a very accurate model. The model discussed in part II of this essay is actually not very different from this approach. After Newton laid out the correct theory of gravity, the subject evolved rapidly. Many famous mathematicians and physicists like Lagrange, who discovered the existence of Lagrangian points, and Newcomb, who made a large contribution to the calculation of ephemerides, developed various techniques of which we will use only a few in this essay.

In 1915, Albert Einstein successfully described the anomalous precession of Mercury's perihelion as a general relativistic effect. In recent years, astronomers observed deviations of the motion of

stars in galaxies from the general relativistic predictions. This led to the discovery of so called dark matter. It is astounding that, until the present day, there are many unsolved problems in celestial mechanics.

2.4 Elliptic Orbit

The classical two-body problem is the simplest non-trivial problem in celestial mechanics. We assume that the two bodies interact only gravitationally, and let the gravitational forces be

$$\begin{aligned}\mathbf{F}_1 &= +G\frac{m_1m_2}{r^3}\mathbf{r} = m_1\ddot{\mathbf{r}}_1 \\ \mathbf{F}_2 &= -G\frac{m_1m_2}{r^3}\mathbf{r} = m_2\ddot{\mathbf{r}}_2,\end{aligned}$$

where m_1, m_2 are the masses of body 1 and 2, respectively, $\mathbf{r}_1, \mathbf{r}_2$ their position vector and \mathbf{r} their relative separation. The sum of the forces vanishes, thus $m_1\ddot{\mathbf{r}}_1 = m_2\ddot{\mathbf{r}}_2$. Integrating this twice gives

$$\begin{aligned}m_1\dot{\mathbf{r}}_1 + m_2\dot{\mathbf{r}}_2 &= \mathbf{a} \\ m_1\mathbf{r}_1 + m_2\mathbf{r}_2 &= \mathbf{a}t + \mathbf{b}\end{aligned}$$

with two constant vectors \mathbf{a}, \mathbf{b} . We can write the position vector of the centre of mass as $\mathbf{R} = (m_1m_2)^{-1} \cdot (m_1\mathbf{r}_1 + m_2\mathbf{r}_2)$. Using the equations for \mathbf{r}_1 and \mathbf{r}_2 above, it follows that \mathbf{R} is a linear function of time. Thus, only the relative motion \mathbf{r} is interesting and we get

$$\frac{d^2\mathbf{r}}{dt^2} + \mu\frac{\mathbf{r}}{r^3} = 0, \quad \mu = G(m_1 + m_2). \quad (2.4)$$

We now switch to polar coordinates centred on body 1. This will become useful as the problem is restricted to a plane. In polar coordinates the position and the acceleration can be written as

$$\mathbf{r} = r\hat{\mathbf{r}} \quad \ddot{\mathbf{r}} = \left(\ddot{r} - r\dot{\theta}^2\right)\hat{\mathbf{r}} + \left(\frac{1}{r}\frac{d}{dt}\left(r^2\dot{\theta}\right)\right)\hat{\theta},$$

where $\hat{\mathbf{r}}$ and $\hat{\theta}$ are unit vectors in the plane. In this coordinate system equation (2.4) becomes a scalar equation

$$\ddot{r} - r\dot{\theta}^2 = -\mu\frac{1}{r^2}.$$

The solutions are the four well known conic section curves: circle, ellipse (see figure 2.1), parabola, hyperbola. The general equation for r is

$$r = \frac{p}{1 + e\cos(\theta - \varpi)}. \quad (2.5)$$

The value of the eccentricity e defines the conic section we are considering as shown in the following table.

conic section	eccentricity e	semilatus rectum p
hyperbola	$e > 1$	$p = a(e^2 - 1)$
parabola	$e = 1$	$p = 2q$
ellipse	$0 < e < 1$	$p = a(1 - e^2)$
circle	$e = 0$	$p = a$

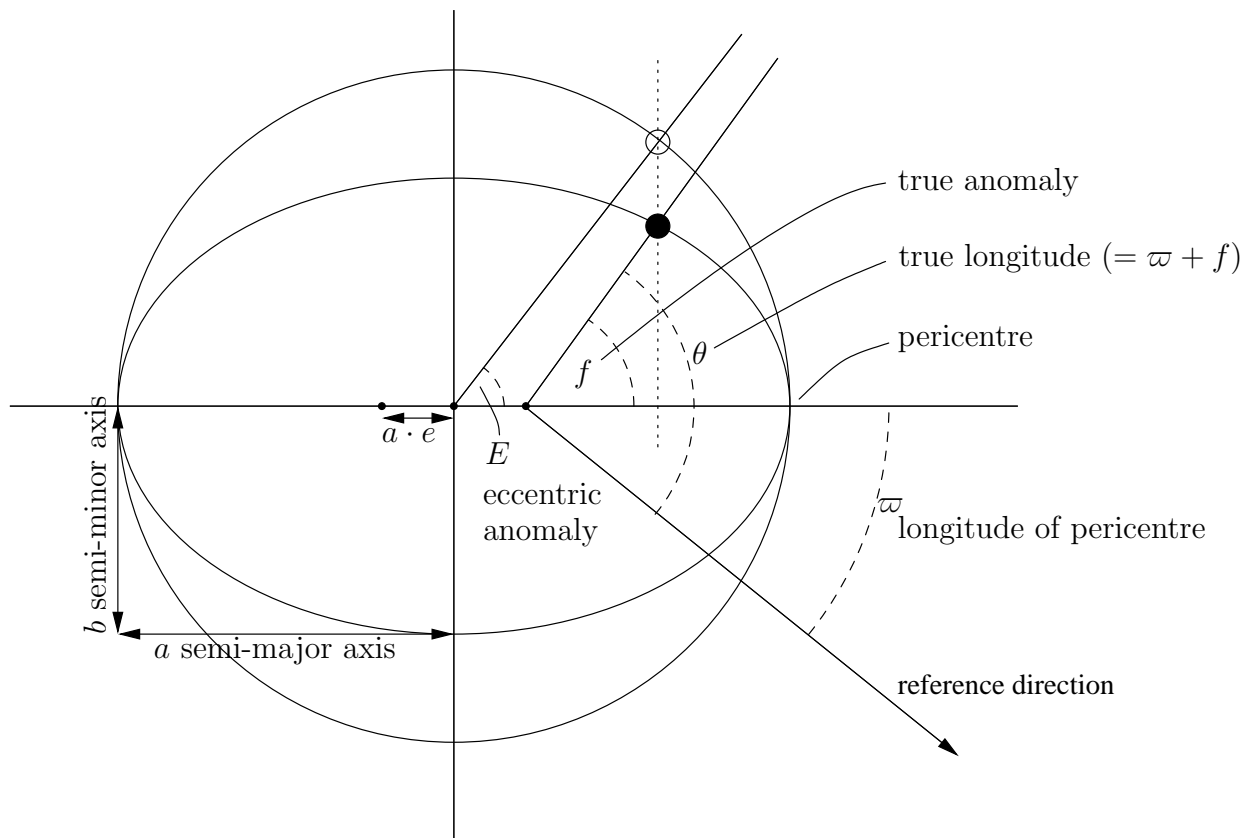


Figure 2.1: Elliptic orbit in a plane. The central object is in a focus of the ellipse, the planet is on the ellipse. The definition of the parameters is given in the text.

The semi-major axis a and the value q are constants. Most bodies in the solar system (except comets) have eccentricities $e \ll 1$. Thus we will focus on the elliptical orbit.

The angle θ is called true longitude, ϖ is the longitude of pericentre. The pericentre is the closest approach of the two bodies. It occurs when $\theta = \varpi$. We can define a new angle f , called the true anomaly by $f = \theta - \varpi$ and rewrite equation (2.5) as

$$r = \frac{a(1 - e^2)}{1 + e \cos f}.$$

The orbital period is $T = 2\pi\sqrt{\frac{a^3}{\mu}}$. The coordinates r and f are non-linear functions of time (in the case $e \neq 0$). We can define a linear function of time M , called the mean anomaly, using the average angular velocity or mean motion $n = 2\pi/T$:

$$M = n(t - \tau).$$

τ is a constant and can be chosen to be the time of pericentre passage. The mean anomaly does not have a simple geometrical interpretation but will become useful later on. The mean longitude λ is the mean anomaly measured not with respect to the pericentre, but to the reference direction in the orbital plane: $\lambda = M + \varpi$. Let us define one more angle, E , called the eccentric anomaly. The eccentric anomaly can be constructed geometrically by a circumscribed circle of radius a around the ellipse (see figure 2.1). The relation between E and M is given by Kepler's equation:

$$M = E - e \sin E. \tag{2.6}$$

Kepler's equation cannot be rearranged to solve for E . This is the reason why it is not possible to determine a planet's position analytically at a given time. However, approximations and numerical methods can solve this problem to arbitrary accuracy.

The orbit is restricted to a two dimensional plane. The plane is arbitrarily oriented and we need two angles to describe it; the inclination i and the angle of the ascending node Ω . The inclination is the angle of the orbital plane with respect to a reference plane, e.g. the xy -plane. The ascending node is the point where the orbit crosses the reference plane and the longitude of the ascending node is measured with respect to an arbitrary reference direction, e.g. the x axis.

Part II

Turbulence and Mean Motion Resonances

Chapter 3

Overview

About 10% of the detected multiple planetary systems are in or very close to a resonant configuration where two planets show a mean motion commensurability, with four systems in or near a 2:1 resonance (??).

As mentioned in previous chapters, those resonant configurations can be established by a dissipative force acting on the planets which lead to convergent migration (see also ??). The magneto rotational instability (MRI, see section 1.4) is thought to be responsible for an anomalous large value of ν which is often characterized using the $\alpha = \nu / (c_s \Omega)$ parameter, with c_s being the local sound speed and $2\pi/\Omega$ being the orbital period. The value of α is uncertain when realistic values of the actual transport coefficients are employed because of numerical resolution issues (see ??). Which parts of protoplanetary discs are adequately ionized, or constitute a dead zone, is also an issue (eg. ?). Because the level of MRI turbulence and associated density fluctuations are very uncertain, we consider stochastic force amplitudes ranging over several orders of magnitude.

The influence of stochastic forces resulting from the gravitational field produced by the density fluctuations associated with MRI turbulence on migrating planets was explored first by ?. They considered MRI simulations directly with the result that only a relatively small number of orbits was considered. To consider much longer evolution times as done here a simpler parameterized model of the forcing is needed. Recently studies (??) looked at lifetimes of mean motion resonances which are perturbed by stochastic kicks. They found that resonances were disrupted within expected disc lifetimes for sufficiently large forcing.

In this essay we expand the discussion, focusing on physical scaling laws and a self consistent analytic model that allows us to predict the form of the dynamical evolution of multi-planetary systems under stochastic forcing. We find that stochastic forcing readily produces systems in mean motion resonance with broken apsidal corotation. This feature is used to construct a scenario involving convergent migration and stochastic forcing to account for the HD128311 system.

The plan of this part of the essay is as follows. In chapter 4 we present the basic equations governing two interacting planets subject to external stochastic forces. We specialize to the case where the planets are either in or near a mean motion commensurability and so retain only the two angle variables that vary on a time scale much longer than the orbital one. Considering the case where these angles undergo small amplitude librations, we identify fast and slow libration modes, the former being associated with variations in the semi-major axes and the latter with the angle between the apsidal lines of the two planets. We go on to consider the effects of stochastic forcing arising from some external process such as disc turbulence in section 4.3

deriving the diffusion rates for the orbital elements of a single planet and the growth rate of the libration amplitudes in the two planet case.

In chapter 5 we discuss the origin and numerical implementation of the stochastic forcing and their operation in the single planet case. In chapter 6 we go on to consider the stochastic forcing in the two planet case. We consider the conversion of the fast and slow modes from libration to circulation for model systems of varying total mass ratio and initial eccentricities including GJ876. The slow mode is found to convert faster through sensitivity to the attainment of small eccentricities and coupling to the fast mode. Investigations are carried out for stochastic diffusion rates, proportional to the mean square stochastic force amplitude ranging over several orders of magnitude. The life time of the resonant angles is found to be inversely proportional to the diffusion rate except in the case of systems with low total mass in the earth mass range. In chapter 7 we exploit the tendency of the slow mode, related to the angle between the apsidal lines, to be driven to circulate while the fast mode still librates in stochastically forced systems, to make a model for the formation of the HD128311 system which may be in such a state, which was not readily understood in terms of convergent migration models for producing the commensurability. We combine the effects of such migration and stochastic forcing, showing that during the migration phase, while the librations tend to be stabilized, the slow mode is readily converted to circulation while the fast mode continues to librate. Good agreement is obtained with the somewhat uncertain observed orbital configuration. Finally in chapter 8 we summarize and discuss our results.

Chapter 4

Basic Equations

We begin by writing down the equations of motion for a single planet moving in a fixed plane under a general Hamiltonian H in the form (see e.g. ??)

$$\dot{E} = -n \frac{\partial H}{\partial \lambda} \quad (4.1)$$

$$\dot{L} = - \left(\frac{\partial H}{\partial \lambda} + \frac{\partial H}{\partial \varpi} \right) \quad (4.2)$$

$$\dot{\lambda} = \frac{\partial H}{\partial L} + n \frac{\partial H}{\partial E} \quad (4.3)$$

$$\dot{\varpi} = \frac{\partial H}{\partial L}. \quad (4.4)$$

Here the angular momentum of the planet is L and the energy is E . For orbital motion around a central point mass M we have

$$L = m \sqrt{GMa(1 - e^2)} \quad \text{and} \quad (4.5)$$

$$E = - \frac{GMm}{2a}, \quad (4.6)$$

where a is the semi-major axis and e is the eccentricity.

The mean longitude is $\lambda = n(t - t_0) + \varpi$, where n the mean motion, with t_0 being the time of periastron passage and ϖ being the longitude of periastron.

4.1 Additional Forcing of a Single Planet

In order to study the phenomena such as stochastic forcing we need to consider the effects of an additional external force per unit mass \mathbf{F} which may not be described using a Hamiltonian formalism. However, as may be seen by considering general coordinate transformations starting from a Cartesian representation, the equations of motion are linear in the components of \mathbf{F} . Because of this we may determine them by considering forces of the form $\mathbf{F} = (F_x, F_y)$ for which the Cartesian components are constant. Having done this we may then suppose that these vary with coordinates and time in an arbitrary manner. Following this procedure we note that when \mathbf{F} , as in the above form is constant, we may derive the equations of motion by replacing the original Hamiltonian with a new Hamiltonian defined through

$$H \rightarrow H - m(F_x x + F_y y) = H - m(\mathbf{r} \cdot \mathbf{F}). \quad (4.7)$$

The additional terms proportional to the components of \mathbf{F} correspond to the Gaussian form of the equations of motion (?).

The various derivatives involving \mathbf{r} can be calculated by elementary means and expressed in terms of E, L, λ and ϖ . One thus finds additional contributions to the equations of motion (4.1) - (4.4), indicated with a subscript F , in the form

$$\dot{L}_F = m \left(\frac{\partial}{\partial \lambda} + \frac{\partial}{\partial \varpi} \right) (\mathbf{r} \cdot \mathbf{F}) = m(\mathbf{r} \times \mathbf{F}) \cdot \hat{\mathbf{e}}_z \quad (4.8)$$

$$\dot{E}_F = mn \frac{\partial}{\partial \lambda} (\mathbf{r} \cdot \mathbf{F}) = m\mathbf{v} \cdot \mathbf{F} \quad (4.9)$$

$$\dot{\varpi}_F = -m \frac{\partial}{\partial L} (\mathbf{r} \cdot \mathbf{F}) \quad \text{or equivalently} \quad (4.10)$$

$$\dot{\varpi}_F = \frac{\sqrt{(1-e^2)}}{nae} \left[F_\theta \left(1 + \frac{1}{1-e^2} \frac{r}{a} \right) \sin f - F_r \cos f \right] \quad (4.11)$$

$$\dot{\lambda}_F = -m \left(\frac{\partial}{\partial L} + n \frac{\partial}{\partial E} \right) (\mathbf{r} \cdot \mathbf{F}) \quad (4.12)$$

$$= \left(1 - \sqrt{1-e^2} \right) \dot{\varpi}_F + \frac{2an}{GM} \mathbf{r} \cdot \mathbf{F}, \quad (4.13)$$

where $f = \theta - \varpi$. Note that from (4.9) we obtain

$$\dot{a}_F = -\frac{2a\dot{n}}{3n} = \frac{2(F_r e \sin f + F_\theta(1 + e \cos f))}{n\sqrt{1-e^2}}. \quad (4.14)$$

and from (4.8) together with (4.9) we obtain

$$\dot{e}_F = \frac{L(2E\dot{L} + L\dot{E})}{G^2 m^3 M^2 e}. \quad (4.15)$$

In the limit $e \ll 1$ this becomes (ignoring terms $O(e)$ and smaller)

$$\dot{e}_F = F_r \frac{1}{an} \sin f + F_\theta \frac{1}{an} 2 \cos f. \quad (4.16)$$

Furthermore in this limit we may replace f by $f = \lambda - \varpi = n(t - t_0)$.

4.2 Multiple Planets

Up to now we have considered a single planet. However, it is a simple matter to generalize the above formalism so that it applies to a system of two planets. Here we follow closely the discussions in ? and ?. Excluding stochastic forcing for the time being, we start from the Hamiltonian formalism describing their mutual interactions using Jacobi coordinates (see ?). In this formalism the radius vector \mathbf{r}_2 , of the inner planet of reduced mass m_2 is measured from M and that of the outer planet, \mathbf{r}_1 , of reduced mass m_1 is referred to the centre of mass of M and m_2 . Thus from now on we consistently adopt a subscripts 1 and 2 for coordinates related to the outer and inner planets respectively.

The required Hamiltonian correct to second order in the planetary masses is given by

$$H = \frac{1}{2}(m_1|\dot{\mathbf{r}}_1|^2 + m_2|\dot{\mathbf{r}}_2|^2) - \frac{GM_1 m_1}{|\mathbf{r}_1|} - \frac{GM_2 m_2}{|\mathbf{r}_2|} - \frac{Gm_1 m_2}{|\mathbf{r}_{12}|} + \frac{Gm_1 m_2 \mathbf{r}_1 \cdot \mathbf{r}_2}{|\mathbf{r}_1|^3}. \quad (4.17)$$

Here $M_1 = M + m_1$, $M_2 = M + m_2$ and $\mathbf{r}_{12} = \mathbf{r}_2 - \mathbf{r}_1$. The Hamiltonian can be expressed in terms of $E_i, L_i, \varpi_i, \lambda_i, i = 1, 2$ and the time t . The energies are given by $E_i = -Gm_iM_i/(2a_i)$, and the angular momenta $L_i = m_i\sqrt{GM_i a_i(1 - e_i^2)}$ with a_i and e_i denoting the semi-major axes and eccentricities respectively. The mean motions are $n_i = \sqrt{GM_i/a_i^3}$.

The Hamiltonian may quite generally be expanded in a Fourier series involving linear combinations of the three angular differences $\lambda_i - \varpi_i, i = 1, 2$ and $\varpi_1 - \varpi_2$ (eg. ??).

Near a first order $p + 1 : p$ resonance, we expect that both $\phi_1 = (p + 1)\lambda_1 - p\lambda_2 - \varpi_2$, and $\phi_2 = (p + 1)\lambda_1 - p\lambda_2 - \varpi_1$, will be slowly varying. Following standard practice (see eg. ??) only terms in the Fourier expansion involving linear combinations of ϕ_1 and ϕ_2 as argument are retained because only these are expected to lead to large long term perturbations.

The resulting Hamiltonian may then be written in the general form $H = E_1 + E_2 + H_{12}$, where

$$H_{12} = -\frac{Gm_1m_2}{a_1} \sum C_{k,l} \left(\frac{a_1}{a_2}, e_1, e_2 \right) \cos(l\phi_1 + k\phi_2), \quad (4.18)$$

where in the above and similar summations below, the sum ranges over all positive and negative integers (k, l) and the dimensionless coefficients $C_{k,l}$ depend on e_1, e_2 and the ratio a_1/a_2 only. We also replace M_i by M .

4.2.1 Equations of Motion

The equations of motion for each planet can now be easily derived that take into account the contributions due to their mutual interactions (see ??) and contributions from (4.8) - (4.13). The latter terms arising from external forcing are indicated with a subscript F . We thus obtain to lowest order in the perturbing masses.

$$\frac{dn_1}{dt} = \frac{3(p+1)n_1^2m_2}{M} \sum C_{k,l}(k+l) \sin(l\phi_1 + k\phi_2) + \left(\frac{dn_1}{dt} \right)_F \quad (4.19)$$

$$\frac{dn_2}{dt} = -\frac{3pn_2^2m_1a_2}{Ma_1} \sum C_{k,l}(k+l) \sin(l\phi_1 + k\phi_2) + \left(\frac{dn_2}{dt} \right)_F \quad (4.20)$$

$$\begin{aligned} \frac{de_1}{dt} &= -\frac{m_2n_1\sqrt{1-e_1^2}}{e_1M} \cdot \sum C_{k,l} \sin(l\phi_1 + k\phi_2) \\ &\cdot \left[k - (p+1)(k+l) \left(1 - \sqrt{1-e_1^2} \right) \right] + \left(\frac{de_1}{dt} \right)_F \end{aligned} \quad (4.21)$$

$$\begin{aligned} \frac{de_2}{dt} &= -\frac{m_1a_2n_2\sqrt{1-e_2^2}}{a_1e_2M} \cdot \sum C_{k,l} \sin(l\phi_1 + k\phi_2) \\ &\cdot \left[l + p(k+l) \left(1 - \sqrt{1-e_2^2} \right) \right] + \left(\frac{de_2}{dt} \right)_F \end{aligned} \quad (4.22)$$

$$\frac{d\phi_2}{dt} = (p+1)n_1 - pn_2 - \sum (D_{k,l} + E_{k,l}) \cos(l\phi_1 + k\phi_2) + \left(\frac{d\phi_2}{dt} \right)_F \quad (4.23)$$

$$\frac{d\phi_1}{dt} = (p+1)n_1 - pn_2 - \sum (D_{k,l} + F_{k,l}) \cos(l\phi_1 + k\phi_2) + \left(\frac{d\phi_1}{dt} \right)_F. \quad (4.24)$$

Here

$$D_{k,l} = \frac{2(p+1)n_1a_1^2m_2}{M} \frac{\partial}{\partial a_1} (C_{k,l}/a_1) - \frac{2pn_2a_2^2m_1}{M} \frac{\partial}{\partial a_2} (C_{k,l}/a_1), \quad (4.25)$$

$$E_{k,l} = \frac{n_1m_2 \left((p+1)(1-e_1^2) - p\sqrt{1-e_1^2} \right)}{e_1M} \frac{\partial C_{k,l}}{\partial e_1} + \frac{pn_2a_2m_1 \left(\sqrt{1-e_2^2} - 1 + e_2^2 \right)}{a_1e_2M} \frac{\partial C_{k,l}}{\partial e_2} \quad (4.26)$$

and

$$F_{k,l} = \frac{(p+1)n_1m_2 \left(1 - e_1^2 - \sqrt{1-e_1^2} \right)}{e_1M} \frac{\partial C_{k,l}}{\partial e_1} + \frac{n_2a_2m_1 \left((p+1)\sqrt{1-e_2^2} - p(1-e_2^2) \right)}{a_1e_2M} \frac{\partial C_{k,l}}{\partial e_2}. \quad (4.27)$$

Note that $\phi_2 - \phi_1 = \varpi_2 - \varpi_1 \equiv \Delta\varpi$ is the angle between the two apsidal lines of the two planets. We also comment that, up to now, we have not assumed that the eccentricities are small and that, in addition to stochastic contributions, the external forcing terms may in general contain contributions from very slowly varying disc tides but we shall not consider these further in this article.

4.2.2 Modes of Libration

We first consider two planets in resonance with no external forces acting in order to identify the possible libration modes. We then consider the effects of the addition of external stochastic forcing. In the absence of external forces equations (4.19) - (4.24) can have a solution for which a_i and e_i are constants and the angles ϕ_1 and ϕ_2 are zero. In general other values for the angles may be possible but such cases do not occur for the numerical examples presented below. When the angles are zero equations (4.23) and (4.24) provide a relationship between e_1 and e_2 (see eg. ?).

We go on to consider small amplitude oscillations or librations of the angles about their above equilibrium state. Because two planets are involved there are two modes of oscillation which we find convenient to separate and describe as fast and slow modes. Assuming the planets have comparable masses, the fast mode has libration frequency $\propto \sqrt{m}$ and the slow mode has libration frequency $\propto m$. These modes clearly separate as the planet masses are decreased while maintaining fixed eccentricities.

4.2.3 Fast Mode

To obtain the fast mode we linearize (4.19) - (4.24) and neglect second order terms in the planet masses. This is equivalent to neglecting the variation of $D_{k,l}$, $E_{k,l}$ and $F_{k,l}$ in equations (4.23) and (4.24) which then require that $\phi_1 = \phi_2$ very nearly for this mode. Differentiation of either of equations (4.23) or (4.24) with respect to time then gives for small amplitude oscillations

$$\frac{d^2\phi_i}{dt^2} + \omega_{lf}^2\phi_i = 0, \quad (i = 1, 2), \quad (4.28)$$

where

$$\omega_{lf}^2 = -\frac{3p^2 n_2^2 m_2}{M} \left(1 + \frac{a_2 m_1}{a_1 m_2}\right) \cdot \sum C_{k,l} (k+l)^2 \quad (4.29)$$

and we have used the resonance condition that $(p+1)n_1 = p_2 n_2$ which is satisfied to within a correction of order $\sqrt{m_1/M}$. Note that for this mode the fact that $\phi_1 = \phi_2$ very nearly, implies that $\varpi_2 - \varpi_1$ is small. Thus that quantity does not participate in the oscillation.

4.2.4 Slow Mode

In this case we look for low frequency librations with frequency $\propto m_1$. Equations (4.23) and (4.24) imply that, for such oscillations, to within a small relative error of order m_1/M , $(p+1)n_1 = p n_2$ throughout.

Equations (4.19) and (4.20) then imply that the two angles are related by $\phi_2 = \beta \phi_1$, where $\beta = -\sum C_{k,l}(k+l)l / (\sum C_{k,l}(k+l)k)$. Subtracting equation (4.24) from equation (4.23), differentiating with respect to time and using this condition results in an equation for $\zeta = \phi_2 - \phi_1 = \varpi_2 - \varpi_1 = \Delta\varpi$

$$\frac{d^2\zeta}{dt^2} + \omega_{ls}^2 \zeta = 0, \quad (4.30)$$

where

$$\omega_{ls}^2 = \alpha_1 \frac{n_1 m_2 \sqrt{1-e_1^2}}{e_1 M (1-\beta)} \frac{\partial W}{\partial e_1} + \alpha_2 \frac{n_2 a_2 m_1 \sqrt{1-e_2^2}}{a_1 e_2 M (1-\beta)} \frac{\partial W}{\partial e_2} \quad (4.31)$$

with

$$\begin{aligned} \alpha_1 &= \sum C_{k,l} \left[k - (p+1)(k+l) \left(1 - \sqrt{1-e_1^2}\right) \right] (k\beta + l), \\ \alpha_2 &= \sum C_{k,l} \left[l + p(k+l) \left(1 - \sqrt{1-e_2^2}\right) \right] (k\beta + l) \end{aligned}$$

and

$$W = \left(\frac{n_1 a_2 m_2 \sqrt{1-e_2^2}}{a_1 e_2 M} \frac{\partial}{\partial e_2} - \frac{n_2 m_1 \sqrt{1-e_1^2}}{e_1 M} \frac{\partial}{\partial e_1} \right) \cdot \sum C_{k,l}.$$

Although the expressions for the mode frequencies are complicated, the fast frequency scales as the square root of the planet mass and the slow frequency scales as the planet mass independent of the magnitude of the eccentricities while both scale as the characteristic mean motion of the system. Furthermore although we have considered small amplitude librations and accordingly obtained harmonic oscillator equations, the treatment can be extended to consider finite amplitude oscillations and generalized pendulum equations as long as the two mode frequencies can be separated. However, we shall not consider this aspect further here.

4.2.5 Librations with External Forcing

When external forcing is included source terms appear on the right hand sides of equations (4.28) and (4.30). We shall assume that the forcing terms are small so that terms involving products of these and the planet masses may be neglected. Then in the case of the slow mode, repeating the derivation given above including the forcing terms, we find that (4.30) becomes

$$\frac{d^2\zeta}{dt^2} + \omega_{ls}^2 \zeta = \frac{d}{dt} (\dot{\varpi}_{2F} - \dot{\varpi}_{1F}). \quad (4.32)$$

The quantities $\dot{\omega}_{iF}$ are readily obtained for each planet from (4.11). From this we see that for small eccentricities, $\dot{\omega}_{iF} \propto 1/e_i$, indicating large effects when e_i is small; a feature that will be discussed below. Nonetheless the form of the source term is quite natural because the slow mode is an oscillation of the angle between the apsidal lines of the two planets.

A similar description may be found for the fast mode. In this case, neglecting terms of the order of the square of the planet masses or higher, one may use equations (4.23) and (4.24) to obtain an equation for $Q \equiv \phi_1$ in the form

$$\frac{d^2 Q}{dt^2} + \omega_{if}^2 Q = \frac{d}{dt} [\dot{\phi}_{1F}] + (p+1)\dot{n}_{1F} - p\dot{n}_{2F}. \quad (4.33)$$

Equations (4.32) and (4.33) form a pair of equations for the stochastically forced fast and slow modes respectively. We comment that this mode separation is not precise. However, it can be made so by choosing appropriate linear combinations of the above modes. Numerical results confirm that Q predominantly manifests the fast mode and ζ the slow mode, so we do not expect such a change of basis to significantly affect conclusions.

We further comment that because ϕ_{1F} contains $\dot{\omega}_{2F}$ but not $\dot{\omega}_{1F}$, for small eccentricities there are only potential forcing terms $\propto 1/e_2$ that occur when forcing is applied to the inner planet. As this planet has the larger eccentricity for the situations we consider, small eccentricities are not found to play any significant role in this case.

Each mode responds as a forced oscillator. We suppose the forcing contains a stochastic component which tends to excite the respective oscillator and ultimately convert libration into circulation. But we stress that the above formulation as well as developments below assume small librations, so we may only assess the initial growth of oscillation amplitude. However, inferences based on the structure of the non linear governing equations and an extrapolation of the linear results enable successful comparison with numerical results.

4.3 Stochastic Forces

We assume that turbulence causes the external force per unit mass (F_r, F_θ) acting on each planet to be stochastic. For simplicity we shall adopt the simplest possible model. Regarding the components of the force, per unit mass expressed in cylindrical coordinates to be a function of time t , we assume any one of these satisfies the relation $F_i(t)F_i(t') = \langle F_i^2 \rangle g(|t - t'|)$ where the autocorrelation function $g(x)$ is such that $\int_0^\infty g(x)dx = \tau_c$, where τ_c is the correlation time and $\sqrt{\langle F_i^2 \rangle}$ is the root mean square value of the i component. It should be noted that an ensemble average is implied on the left hand side. Again for simplicity we assume that different components acting on the same planet as well as components acting on different planets are uncorrelated. We note that in general the root mean square values as well as τ_c may depend on t , but we shall not take this into account here and simply assume that these quantities are constant.

We note the stochastic forces make quantities they act on undergo a random walk. Thus if for example $\dot{A} = F_i$ for some quantity A (note that constants or slowly varying quantities originally multiplying F_i may be absorbed by a redefinition of A and so do not materially affect the discussion given below), the square of the change of A occurring after a time interval t is

given by

$$\begin{aligned}
(\Delta A)^2 &= \int_0^t \int_0^t F_i(t') F_i(t'') dt' dt'' \\
&= \int_0^t \int_0^t \langle F_i^2 \rangle g(|t' - t''|) dt' dt'' \rightarrow D_i t,
\end{aligned} \tag{4.34}$$

Here we take the limit where t/τ_c is very large corresponding to an integration time of very many correlation times and

$D_i = 2 \langle F_i^2 \rangle \tau_c$ is the diffusion coefficient.

When the evolution of a stochastically forced planetary orbit is considered, it is more appropriate to consider a model governing equation for A of the generic form

$$\dot{A} = F_i \sin(nt), \tag{4.35}$$

where we recall that $2\pi/n$ is the orbital period (but note that a different value could equally well be considered). We note in passing that, by shifting the origin of time, an arbitrary phase may be added to the argument of the sin without changing the results given below. One readily finds that equation (4.34) is replaced by

$$\begin{aligned}
(\Delta A)^2 &= \int_0^t \int_0^t F_i(t') F_i(t'') \sin(nt') \sin(nt'') dt' dt'' \\
&= \int_0^t \int_0^t \langle F_i^2 \rangle g(|t' - t''|) \sin(nt') \sin(nt'') dt' dt'' \rightarrow \frac{\gamma Dt}{2},
\end{aligned} \tag{4.36}$$

where $\gamma(n) = \int_0^\infty g(x) \cos(nx) dx$.

Note that when $n\tau_c \ll 1$, corresponding to the correlation time being much less than the orbital period, $\gamma \rightarrow 1$. For larger τ_c , $\gamma < 1$ gives a reduction factor for the amount of stochastic diffusion. For example if we adopt an exponential form for the autocorrelation function such that

$$g(|t' - t''|) = \exp\left(-\frac{|t' - t''|}{\tau_c}\right),$$

we find

$$\gamma = \frac{1}{1 + n^2 \tau_c^2} \tag{4.37}$$

and for the purposes of comparison with numerical work we shall use this from now on.

4.3.1 Stochastic Forcing of an Isolated Planet

We begin by considering the effect of stochastic forcing on a single isolated planet. In this case we may obtain a statistical estimate for the characteristic growth of the orbital parameters as a function of time by integrating equations (4.9), (4.11) and (4.16) with respect to time directly. We may then apply the formalism leading to the results expressed in generic form through equations (4.34) - (4.37) to obtain estimates for the stochastic diffusion of the orbital elements in the limit of small eccentricity in the form

$$(\Delta a)^2 = 4 \frac{Dt}{n^2} \tag{4.38}$$

$$(\Delta e)^2 = 2.5 \frac{\gamma Dt}{n^2 a^2} \tag{4.39}$$

$$(\Delta \varpi)^2 = \frac{2.5 \gamma Dt}{e^2 n^2 a^2}. \tag{4.40}$$

4.3.2 Stochastic Variation of the Resonant Angles in the Two Planet Case

We now consider the effects of stochastic forcing on the resonant angles. While the libration amplitude is small enough for linearization to be reasonable, the evolution is described by equations (4.32) and (4.33). These may be solved by the method of variation of parameters. Assuming the amplitude is zero at $t = 0$, the solution of equation (4.32) is given by

$$\zeta = \sin(\omega_{ls}t) \int_0^t \frac{S_\zeta \cos(\omega_{ls}t)}{\omega_{ls}} dt - \cos(\omega_{ls}t) \int_0^t \frac{S_\zeta \sin(\omega_{ls}t)}{\omega_{ls}} dt, \quad (4.41)$$

where $S_\zeta = d(\ddot{\varpi}_{2F} - \ddot{\varpi}_{1F})/dt$. There is a corresponding expression that can be obtained from equation (4.33) is for Q .

Equation (4.41) may be regarded as describing a harmonic oscillator whose amplitude varies in time such that the square of the amplitude after a time interval t is given by

$$(\Delta\zeta)^2 = \left(\int_0^t \frac{S_\zeta \sin(\omega_{ls}t)}{\omega_{ls}} dt \right)^2 + \left(\int_0^t \frac{S_\zeta \cos(\omega_{ls}t)}{\omega_{ls}} dt \right)^2. \quad (4.42)$$

The expression corresponding to this that is obtained from equation (4.33) is

$$(\Delta Q)^2 = \left(\int_0^t \frac{S_Q \sin(\omega_{lf}t)}{\omega_{lf}} dt \right)^2 + \left(\int_0^t \frac{S_Q \cos(\omega_{lf}t)}{\omega_{lf}} dt \right)^2, \quad (4.43)$$

where $S_Q = d(\dot{\phi}_{1F})/dt + (p+1)\dot{n}_{1F} - p\dot{n}_{2F}$.

We now evaluate the expectation values of these using the formalism of section 4.3. For simplicity and as considered numerically later we shall specialize to the case when stochastic forces act only on the outer planet (but see section 8 below). Taking equation (4.42), we perform an integration by parts neglecting the end point contribution as these are associated with subdominant contributions increasing less rapidly than t for large t , to obtain

$$(\Delta\zeta)^2 = \left(\int_0^t \ddot{\varpi}_{1F} \sin(\omega_{ls}t) dt \right)^2 + \left(\int_0^t \ddot{\varpi}_{1F} \cos(\omega_{ls}t) dt \right)^2. \quad (4.44)$$

In dealing with equation (4.43) we neglect $\dot{\phi}_{1F}$ in S because after integration by parts this leads to a contribution on the order ω_{lf}/n smaller than that derived from \dot{n}_{1F} . Thus we simply obtain

$$\frac{(\Delta Q)^2}{(p+1)^2} = \left(\int_0^t \frac{\dot{n}_{1F} \sin(\omega_{lf}t)}{\omega_{lf}} dt \right)^2 + \left(\int_0^t \frac{\dot{n}_{1F} \cos(\omega_{lf}t)}{\omega_{lf}} dt \right)^2. \quad (4.45)$$

We now follow the procedures outlined in section 4.3, working the limit of a small eccentricity, e_1 (but not necessarily e_2), obtaining

$$\frac{(\Delta Q)^2}{(p+1)^2} = \frac{9D\gamma_f t}{a_1^2 \omega_{lf}^2} \quad \text{and} \quad (4.46)$$

$$(\Delta\zeta)^2 = \frac{5D\gamma_s t}{4a_1^2 n_1^2 e_1^2}, \quad (4.47)$$

where

$$\gamma_f = \frac{1}{1 + \omega_{lf}^2 \tau_c^2} \quad \text{and} \quad (4.48)$$

$$\gamma_s = \frac{1}{1 + (n_1 + \omega_{ls})^2 \tau_c^2} + \frac{1}{1 + (n_1 - \omega_{ls})^2 \tau_c^2}. \quad (4.49)$$

4.3.3 Growth of Libration Amplitudes

Equations (4.46) and (4.47) express the expected growth of the resonant angle libration amplitudes as a function of time. We remark that these expressions can be simply related to those obtained for a single planet. Thus equations (4.46) and (4.38) applied to the outer planet imply that

$(\Delta Q)^2/(\Delta a_1)^2 = 9(p+1)^2 n_1^2 \gamma_f / (4a_1^2 \omega_{1f}^2)$. As we are interested in the case $p = 1$, the width of the libration zone is $\sim a_1 \omega_{1f} / n_1$, we see that the time for $(\Delta Q)^2$ to reach unity is comparable for the semi-major axis to diffuse through the libration zone.

Similarly equation (4.47) for $(\Delta \zeta)^2$ gives almost the same result as that for $(\Delta \varpi_1)^2$ obtained from equation (4.40) applied to the outer planet. This indicates that ζ being the angle between the apsidal lines of the two planets diffuses in the same way as for an isolated outer planet subject to stochastic forces. Thus, in the small amplitude regime, the way this diffusion occurs would appear to be essentially independent of whether the planets are in resonance (but see below).

An important feature of equation (4.47) for $(\Delta \zeta)^2$, in this context, is its proportionality to $1/e_1^2$. The latter quantity was assumed constant in the analysis. However it also undergoes stochastic diffusion (see equation (4.39)) as well as oscillations through its participation in libration. Should e_1^2 attain *very small* values through this process, then from (4.47) we expect the onset of a rapid diffusion of ζ . Accordingly the attainment of circulation for this angle, should be related to the diffusion of e_1^2 allowing very small values of that quantity to be attained, rather than the direct excitation of libration amplitude. This is particularly the case when e_1^2 starts from relatively small values.

In fact application of (4.47) and (4.46) to the numerical examples discussed below, indicates that the diffusion of ζ is significantly smaller than Q unless e_1 starts out with a very small value. This would suggest that Q reaches circulation before ζ . However, this neglects the coupling between the angles that occurs once the libration amplitudes become significant. It is readily seen that it is not expected that Q could circulate while ζ remains librating as it was initially. One expects to recover standard secular dynamics for ζ from the governing equations (4.19) - (4.23), when these are averaged over an assumed $Q = \phi_1$ circulating with constant \dot{Q} . As a libration of the initial form would not occur under those conditions, we expect, and find, large excursions or increases in the libration amplitude of ζ to be correlated with increases in the libration amplitude of Q . This in turn increases the oscillation amplitude of the eccentricity e_1 , allowing it to pass through zero. The consequent rapid diffusion of ζ then enables it to pass to circulation. Thus the breaking of resonance is ultimately found to be controlled by the excitation of large amplitude librations for $Q = \phi_1$, which induce ζ to pass to circulation somewhat before Q itself.

Chapter 5

Numerical Simulations

We have performed numerical simulations of one and two planet systems that allow for the incorporation of additional stochastic forces with the properties described above. These in turn provide a simple prescription for estimating the effects of stochastic gravitational forces produced by density fluctuations associated with disc turbulence. Results have been obtained using both a fifth order Runge Kutta method and the Bulirsch Stoer method (see section 2.2) with fixed as well as adaptive timesteps. We have checked that results are converged and thus do not actually depend on the integrator used.

First we discuss the expected scaling of the stochastic forces with the physical parameters of the disc and their implementation in the n-body integrations. In order to clarify the physical mechanisms involved and to check the analytic predictions for stochastic diffusion given by equations (4.38) - (4.40) we consider simulations of a single planet undergoing stochastic forcing first. We then move on to consider two planet commensurable systems with and without stochastic forcing. We focus on the way a 2:1 commensurability, corresponding to $p = 1$ is disrupted, highlighting the various evolutionary stages a system goes through as it evolves from a state with a strong commensurability affecting the interaction dynamics, to one where the commensurability is completely disrupted and in some cases a strong scattering occurs. We consider a range of different planet masses and eccentricities (see table 5.1).

5.1 Stochastic Forces

In order to mimic the effects of turbulence, for example produced by the MRI, it is necessary to calibrate these forces with reference to MHD simulations. As described above, the basic parameters characterising the prescription for stochastic forcing that we have implemented are the root mean square value of the force components per unit mass (in cylindrical coordinates)

$\sqrt{\langle F_i^2 \rangle}$ and the auto correlation time τ_c .

From our analytic considerations, we concluded the stochastic forces make the orbital parameters undergo a random walk that is dependent on the force model primarily through the diffusion coefficient $D = 2 \langle F_i^2 \rangle \tau_c$.

For planets under the gravitational influence of a protoplanetary disc, the natural scale for the force per unit mass components, F_i , is $F_0(r) = \pi G \Sigma(r)/2$, where Σ is the characteristic disc surface density (see eg. ?). We comment that $F_0(r)$ is the gravitational force per unit mass due to a small circular disc patch of radius r_Σ at a distance $\sqrt{2} r_\Sigma$ from its centre assuming that all its mass is concentrated there. The result is independent of r_Σ . The natural correlation time τ_c is the inverse of the orbital angular frequency $\tau_{c,0} = \Omega^{-1}$. To set the natural scale for D , we

Planet	m (M_J)	a (AU)	P (days)	e	ζ
GJ876 c	0.790	0.131	30.46	0.263	10°
b	2.530	0.208	60.83	0.031	
GJ876 LM c	0.13	0.131	30.46	0.263	10°
b	0.42	0.208	60.83	0.031	
GJ876 SE c	0.013	0.131	30.46	0.263	10°
b	0.042	0.208	60.83	0.031	
GJ876 E c	0.0013	0.0131	30.46	0.263	10°
b	0.0042	0.208	60.83	0.031	
GJ876 LM HE c	0.13	0.131	30.46	0.41	10°
b	0.42	0.208	60.83	0.09	
GJ876 SE HE c	0.013	0.131	30.46	0.41	10°
b	0.042	0.208	60.83	0.09	
HD128311 b	1.56	1.109	476.8	0.38	58°
c	3.08	1.735	933.1	0.21	

Table 5.1: Parameters of the model systems considered. The first has orbital elements taken from the three planet fit to GJ876 with orbital inclination to the plane of the sky, $i = 50^\circ$ (?). However, the low mass planet GJ876 d is not included. For this system and all others listed here other than the final one, the mass of the central star was taken to be $M_* = 0.38 M_\odot$. The table entries labelled as LM, SE and E have the same parameters as the first entry but the planet masses are scaled down by constant factors of 6, 60, and 600, such that their masses are in the Jovian, Super Earth and terrestrial range respectively. Systems with the added label HE have larger orbital eccentricities. The final entry is a system with the observed elements of HD128311 (?). In this case $M_* = 0.8 M_\odot$.

adopt a minimum mass solar nebula model (MMSN, see ?) with

$$\Sigma(r) = 4200 \frac{\text{g}}{\text{cm}^2} \left(\frac{r}{1 \text{ AU}} \right)^{-3/2}. \quad (5.1)$$

This provides a natural scale for D as a function of the local disc radius and the central stellar mass through

$$D_0 = 2CF_0^2\tau_{c,0} = 25 C \frac{\text{cm}^2}{\text{s}^3} \left(\frac{r}{1 \text{ AU}} \right)^{-3/2} \left(\frac{M_*}{1 M_\odot} \right)^{-1/2}, \quad (5.2)$$

where C is a dimensionless constant.

There are several very uncertain factors which contribute to determining an appropriate value of the dimensionless constant C : The density fluctuations found in MRI simulations are typically $\delta\rho/\rho = \delta\Sigma/\Sigma \approx 0.1$ (eg. ?). The presence of a dead zone in the mid plane regions of the disc, where the MRI is not active, has been found to cause reductions in the magnitude of F_0 by one order of magnitude or more, as compared to active cases (?). Massive planets open a gap in the disc. ? found that most of the contribution to the stochastic force comes from density fluctuations within a distance of one scaleheight from the planet. When a gap forms, this region is cleared of material leading to the expectation of a substantial decrease in the the magnitude of turbulent density fluctuations. Consequently F_0 should be reduced on account of a lower ambient surface density. A factor of $\frac{1}{10}$ seems reasonable although it might be even smaller (?). The correlation time τ_c is actually found to be approximately $0.5\Omega^{-1}$ (??) .

If it is appropriate to include reduction factors to account for all of the above effects, one finds $C = 5 \cdot 10^{-7}$ and we expect a natural scale for the diffusion coefficient to be specified through

$$D_0 \rightarrow 10^{-5} \left(\frac{r}{1 \text{ AU}} \right)^{-3/2} \left(\frac{M_*}{1 M_\odot} \right)^{-1/2} \frac{\text{cm}^2}{\text{s}^3}. \quad (5.3)$$

The same value of D may be equivalently scaled to the orbital parameters of the planets without reference to the disc by writing

$$D_0 = 3.5 \cdot 10^6 \left(\frac{r}{1 \text{ AU}} \right)^{-5/2} \left(\frac{M_*}{1 M_\odot} \right)^{3/2} \cdot \left(\frac{r^4 \langle F_i^2 \rangle \Omega \tau_c}{(GM_*)^2} \right) \frac{\text{cm}^2}{\text{s}^3}. \quad (5.4)$$

Thus a value $D_0 = 10^{-5}$ in cgs units corresponds to a ratio of the root mean square stochastic force component to that due to the central star of about $\sim 10^{-6}$ for a central solar mass at 1 AU. It is a simple matter to scale to other locations.

Of course we emphasize that the value of this quantity is very uncertain, a situation that is exacerbated by its proportionality to the square of the magnitude of the stochastic force per unit mass. For this reason we perform simulations for a range of D covering many orders of magnitude.

5.2 Numerical Implementation

The procedure we implemented, uses a discrete first order Markov process to generate a correlated noise that is continuous and added as an additional force. The Markov process is a statistical process which is defined by two parameters, the root mean square of the amplitude and the correlation time τ_c (?). It has a zero mean value and has no memory. This has the advantage that previous values do not need to be stored. The autocorrelation function decays exponentially and thus mimics the autocorrelation function measured in MHD simulations by ?.

5.3 Stochastic Forces Acting on a Single Planet

We first investigate the long term effect of stochastic forces on a single isolated planet. The initial orbital parameters were taken to be the the observed parameters of GJ876 b (see table 5.1) and the central star had a mass of $0.38 M_{\odot}$. The diffusion coefficient scale D_0 is

$$D_0 = D_{0,\text{GJ876b}} = 3400 \frac{\text{cm}^2}{\text{s}^3}. \quad (5.5)$$

In this simulation, we use the reduced values

$$D = 8.2 \cdot 10^{-5} \frac{\text{cm}^2}{\text{s}^3} \quad \text{and} \quad D = 8.2 \cdot 10^{-3} \frac{\text{cm}^2}{\text{s}^3} \quad (5.6)$$

which can be represented by a correlation time of half the orbital period and a specific force with root mean square values $\sqrt{\langle F^2 \rangle} = 4.05 \cdot 10^{-6} \text{ cm/s}^2$ and $\sqrt{\langle F^2 \rangle} = 4.05 \cdot 10^{-5} \text{ cm/s}^2$, respectively (see also equation (5.4) above).

The resulting random walks undergone by e , a and ϖ are plotted in figure 5.1 for six different realisations for each of the two diffusion parameters. The spreading rates can be estimated from equations (4.38) - (4.40). These analytic predictions are plotted as solid lines. Clearly the numerical model is in broad agreement with the random walk description with a spreading that scales with D as expected. We have performed simulations for a variety of D and get results that are fully consistent with this in all cases.

5.4 Illustration of the Modes of Libration in a Two Planet System

We now go on to consider two planet systems. As an illustrative example we consider the GJ876 system (see table 5.1). Note that we can easily scale all physical quantities and extend the discussion to other systems (see section 8 for a discussion). We begin by considering the evolution of the system without stochastic forcing in order to characterize the modes of libration of the resonant angles and other orbital parameters. In particular we identify the fast and slow modes discussed in section 4.2.2.

The time evolution of the resonant angles and the eccentricities is plotted in figure 5.2. Clearly visible are the slow and fast oscillation modes. The fast mode, which is seen to have a period of about 1.4 years, dominates the librations of e_2 , and ϕ_1 while also being present in those of ϕ_2 . On the other hand the slow mode, which is seen to have a period of about 10 years, dominates the librations of ζ while also being present in those of e_1 and ϕ_2 .

We emphasize the fact that the eccentricities of the two planets participate in the librations and so are not constant. In particular, the eccentricity of GJ876 b oscillates around a mean value of 0.03 with an amplitude $\Delta e \approx 0.01 - 0.02$. This behaviour involving the attainment of smaller values of the eccentricity has important consequences for stochastic evolution as discussed above (see section 4.3.3) and see also below.

We remark that similar behaviour occurs for all the systems we have studied, these have a wide range of eccentricities and planet masses. Indeed we note that the period scalings of the fast and slow mode periods with the planet masses are provided by equations (4.29) and (4.31) respectively. These indicate, as confirmed by our simulations, that if both masses are reduced by a factor Λ then the period of the fast mode scales as $\sqrt{\Lambda}$ and the period of the slow mode scales as Λ .

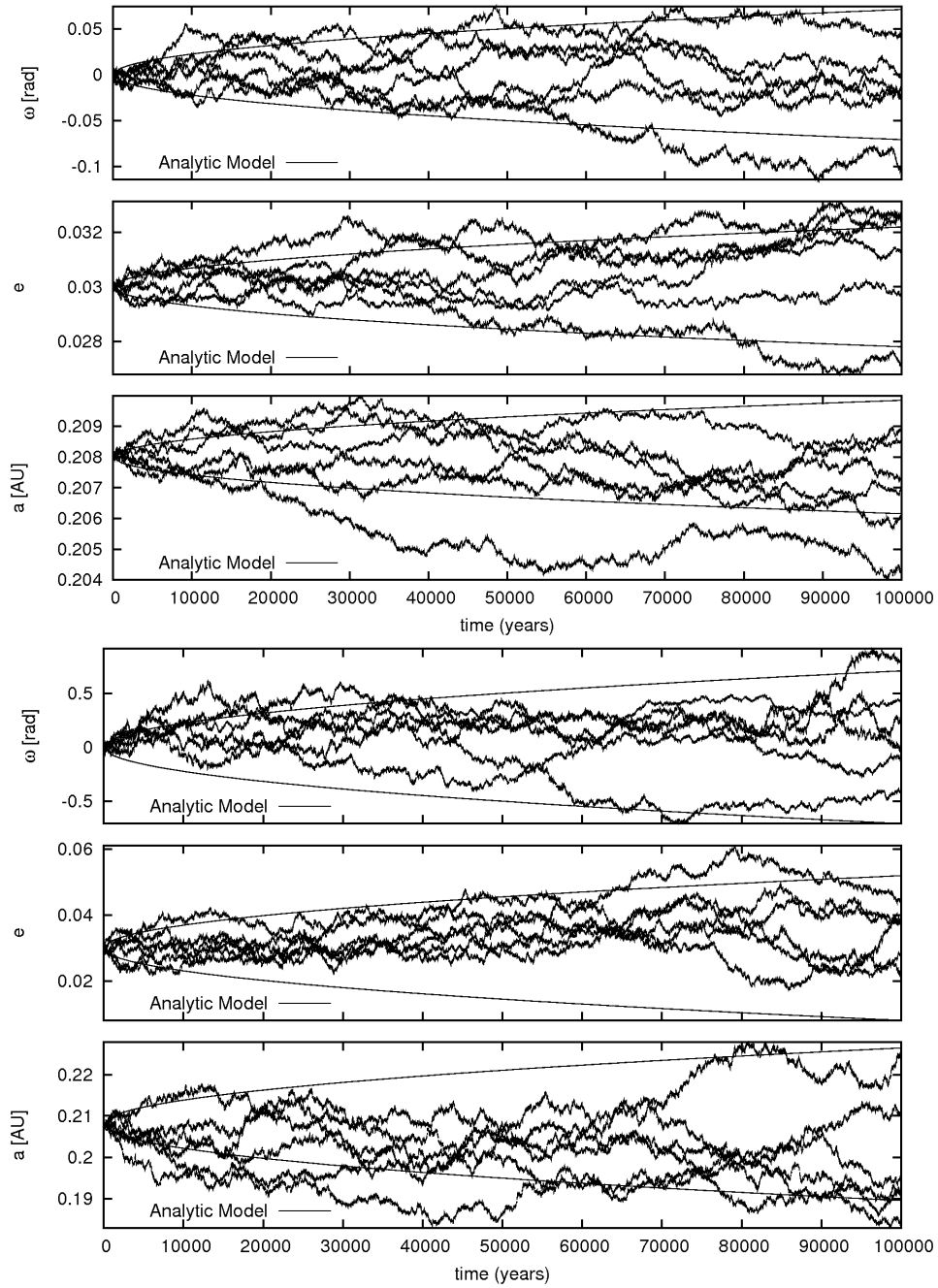


Figure 5.1: Time evolution of the longitude of periastron ϖ , the eccentricity e and the semi major axis a for a single planet. The initial orbital parameters of the planet were taken to be those of GJ876 b (see table 5.1). Six different realisations starting from the same initial conditions are shown in each panel. The diffusion coefficients are $D = 8.2 \cdot 10^{-5} \text{cm}^2/\text{s}^3$ for the upper three panels and $D = 8.2 \cdot 10^{-3} \text{cm}^2/\text{s}^3$ for the lower three respectively. The solid lines correspond to the analytic predictions for the amount of spreading (see text).

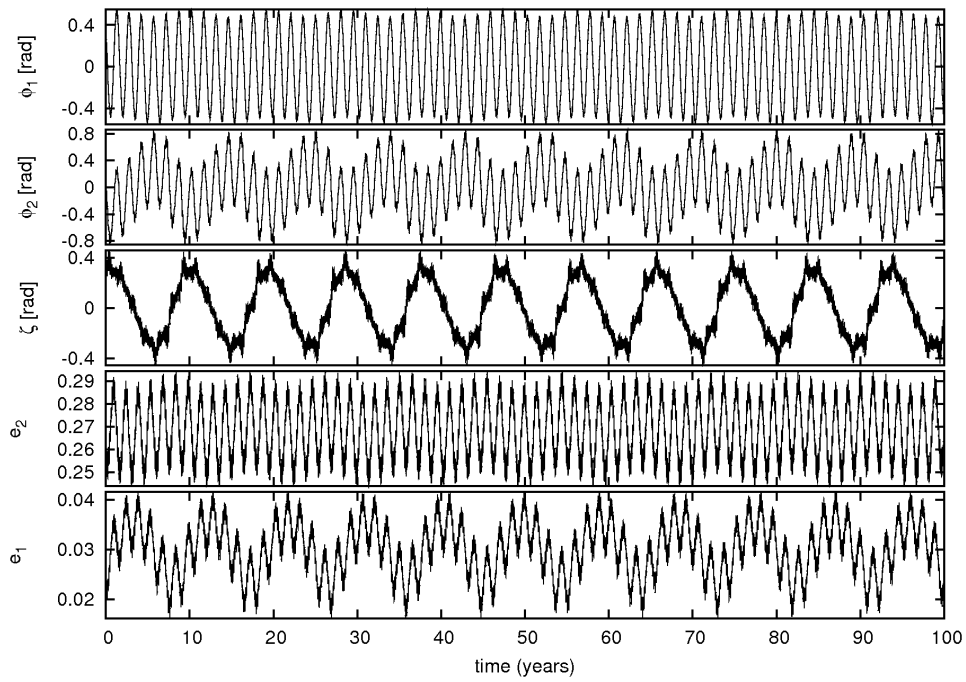


Figure 5.2: Time evolution of the resonant angles and the eccentricities in the system GJ876 without turbulent forcing. The dominance of the fast mode with period ~ 1.4 years in the oscillations of ϕ_1 , and the dominance of the slow mode with period ~ 10 years in ζ can be clearly seen.

Chapter 6

Two Planets with Stochastic Forcing

We now consider systems of two planets with stochastic forcing. For simplicity we begin by applying forcing only to the outer planet. We have found that adding the same form of forcing to the inner planet tends to speed up the evolution by approximately a factor of two without changing qualitative details. For illustrative purposes we again start with the GJ876 system and consider two diffusion coefficients $D = 8.2 \cdot 10^{-5} \text{cm}^2/\text{s}^3$ and $D = 8.2 \cdot 10^{-4} \text{cm}^2/\text{s}^3$. We remark that all of our simulations were run with constant values of $D = 2\langle F_i \rangle^2 \tau_c$. This was done maintaining the parameters $\langle F_i \rangle$ and τ_c to be constant, with τ_c being determined for the initial location of the outer planet. For the cases considered here, there is little orbital migration so this is not a significant feature. Note also that different realizations of the system are likely to become unstable and scatter for higher values of D (see below).

The time evolution of the eccentricities is plotted in figure 6.1. We see fast oscillations superimposed on a random walk. The amplitude of the oscillations, as well as the mean value, changes with time.

Our simple analytic model, assumes slowly changing background eccentricities and semi-major axes and accordingly does not incorporate the oscillations of the eccentricity due to the resonant interaction of the planets. In order to make a comparison, we perform a time average over many periods to get smoothed quantities whose behaviour we can compare with that expected from equations (4.38) - (4.40). When this procedure is followed, the evolution is in reasonable accord with that expected from the analytic model provided that allowance is made for the importance of small values of e_1 in determining the growth of the libration amplitude of the angle between the apsidal lines of the two planets (see equation (4.40)). The presence of this feature results in the behaviour of the libration amplitude being more complex than that implied by a process governed by a simple diffusive random walk.

6.1 Disruption of a Resonance in Stages

Systems with mean motion commensurabilities can be in many different configurations. Here we describe the important evolutionary stages as they appear in a stochastically forced system that starts from a situation in which all the resonant angles show small amplitude libration. For example observations of GJ876 suggest that the system is currently in such a state with the ratio of the orbital periods P_1/P_2 oscillating about a mean value of 2.

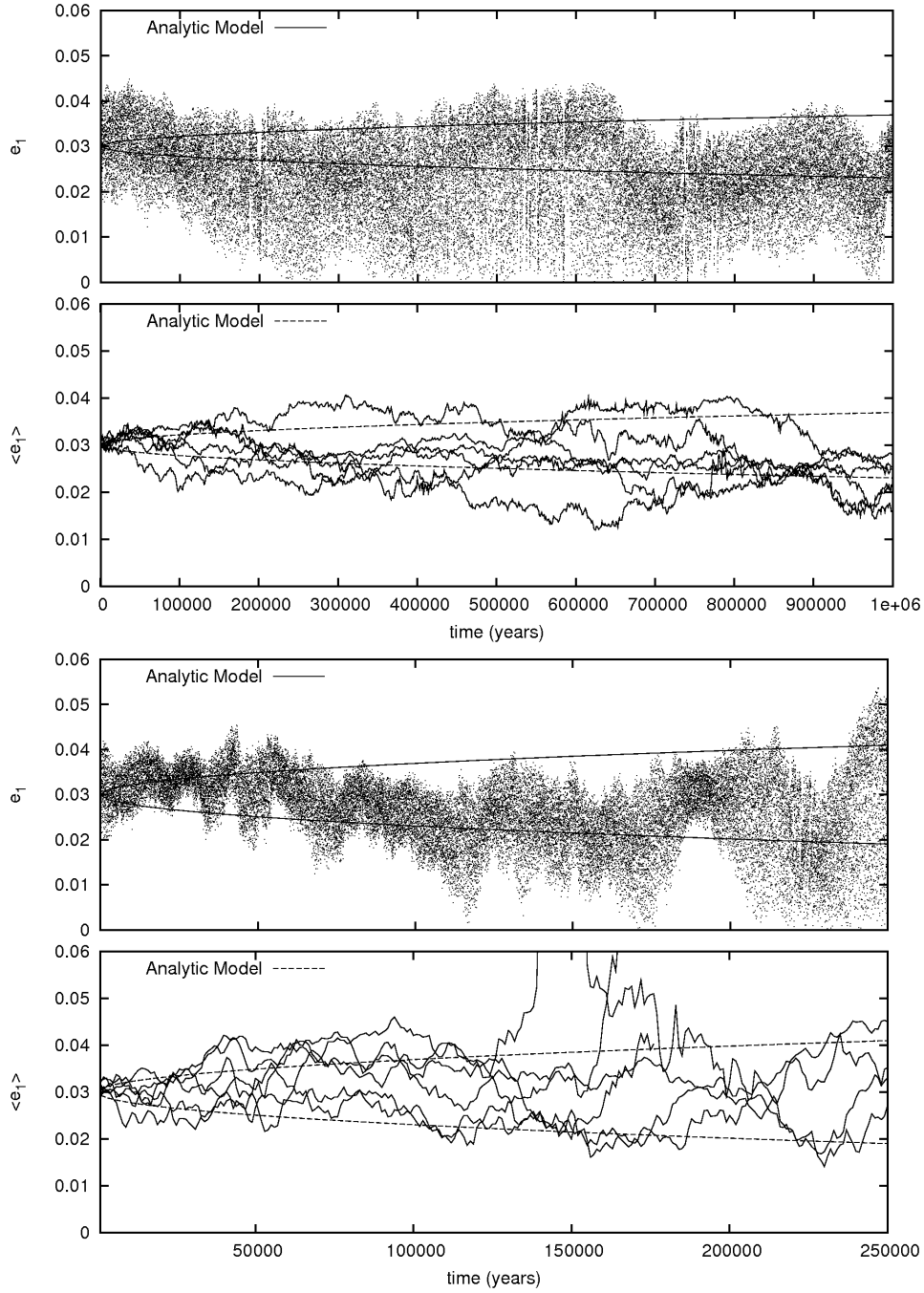


Figure 6.1: Time evolution of the eccentricities in the GJ876 system with turbulent forcing included. The diffusion coefficient is $D = 8.2 \cdot 10^{-5} \text{cm}^2/\text{s}^3$ for the two upper plots and $D = 8.2 \cdot 10^{-4} \text{cm}^2/\text{s}^3$ for the two lower plots. The first (uppermost) and the third plots each show a single run. The second and fourth (lowermost) plots show the time averaged eccentricity for four runs. The averaging interval is 1000 years.

6.1.1 Attainment of Circulation of the Angle Between the Apsidal Lines

When the initial eccentricity of the outer planet, e_1 , is small the excitation of the libration amplitudes of the resonant angles readily bring about a situation where e_1 attains very small values. This causes the periastron difference ζ to undergo large oscillations and eventually circulation (see equation (4.40)). Should stochastic forces cause e_1 to reach zero, ϖ_1 becomes undefined. Subsequently very small perturbations are able to produce a small eccentricity with ζ undergoing large amplitude librations or circulation (see below). Note that the occurrence of this phenomenon does not imply the system ceases to be in a commensurability.

In this context we note that the eccentricity of GJ876 b initially is such that $e_1 \sim 0.03$ with values $e_1 \sim 0.01$ often being attained during libration cycles. Thus only a small change may cause the above situation to occur. In all cases we have considered, we find that ζ enters circulation prior to the fast angle ϕ_1 , which may remain librating until that too is driven into circulation.

6.1.2 Attainment of Circulation of the Fast Angle

Both before and after ζ enters circulation, stochastic forcing acts to increase the libration amplitude of the fast mode. This mode dominates both the librations of the resonant angle ϕ_1 and the semi major axes. Eventually ϕ_1 starts circulation. Shortly afterwards commensurability is lost and P_1/P_2 starts to undergo a random walk with a centre that drifts away from 2. Note that it is possible for some realizations to re-enter commensurability. For systems with the masses of the observed GJ876 system, the most likely outcome is a scattering event that causes complete disruption of the system.

6.1.3 A Numerical Illustration

In order to illustrate the evolutionary sequence described above we plot results for two realisations of the evolution of the GJ876 system in figure 6.2. For these runs we adopted the diffusion coefficient $D = 0.42\text{cm}^2/\text{s}^3$. In this context we note that reducing D increases the evolutionary time which has been found, both analytically and numerically to be $\propto 1/D$ (see below).

The times at which the transition from libration to circulation occurs for both the slow and fast angles are indicated by the vertical lines in figure 6.2. Several of the features discussed above and in section 4.3.3 can be seen in figure 6.2. In particular the tendency for the occurrence of very small values of e_1 to be associated with transitions to circulation of ζ can be seen for the realisation plotted in the lower panels at around $t = 80$ years and $t = 500$ years. Such episodes always seem to occur when the libration amplitude of the fast angle ϕ_1 is relatively boosted, indicating that this plays a role in boosting the slow angle. If the period of time for which e_1 attains small values is small and ϕ_1 recovers small amplitude librations, the slow angle returns to circulation. Thus the attainment of long period circulation for the slow angle is related to the diffusion time for ϕ_1 . We also see from figure 6.2 that the angle ϕ_2 , which has a large contribution from the slow mode, behaves in the same way as ζ as far as libration/circularization is concerned. We have verified by considering the results from the simulations of GJ876 LM HE, which started with a larger value of e_1 , that, as expected, the attainment of circulation of the slow angle takes relatively longer in this case, the time approaching more closely the time when ϕ_1 attains circulation. Also as expected, the time when ϕ_1 attains circulation is not affected by the change in e_1 .

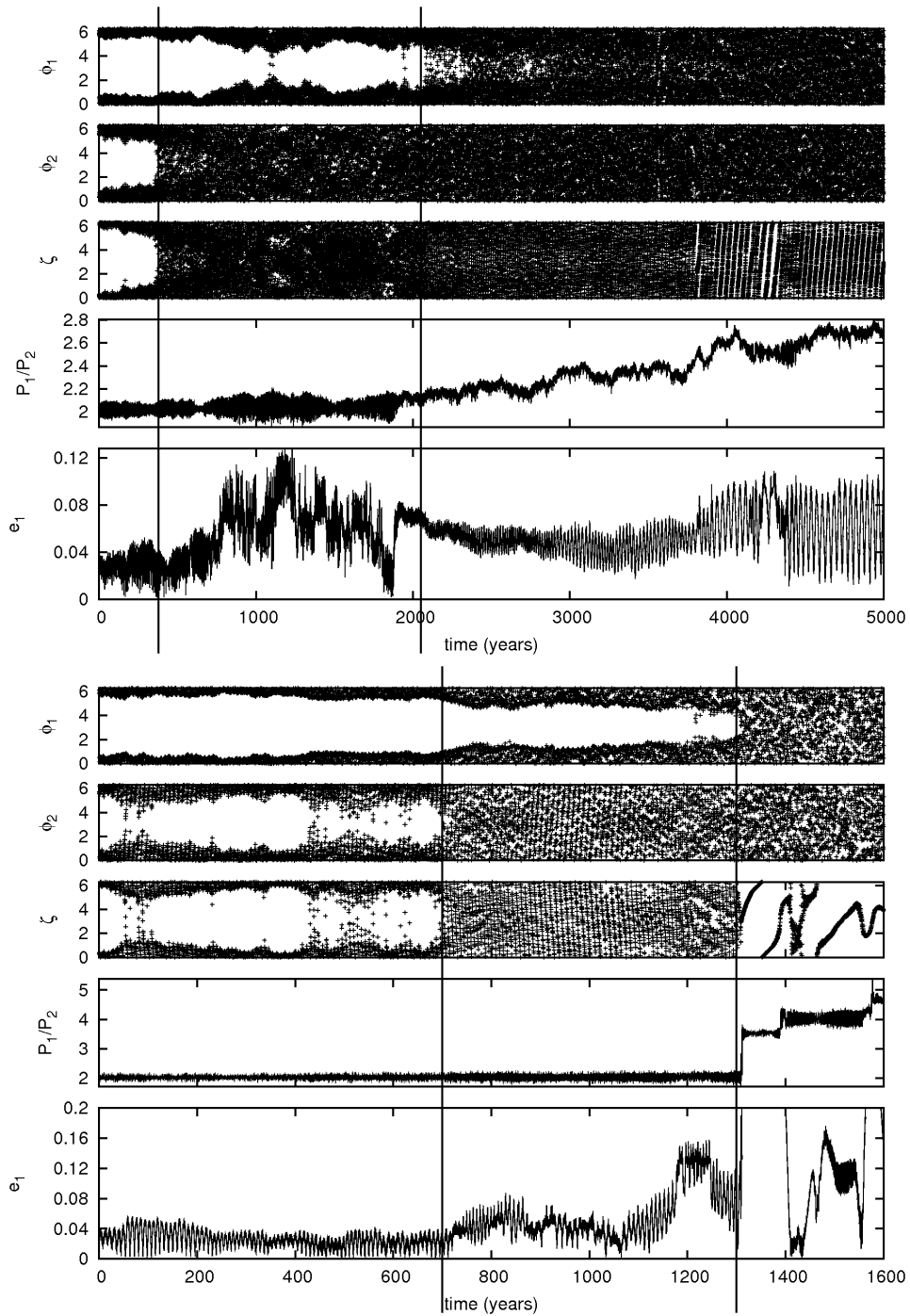


Figure 6.2: Time evolution of the resonant angles, the period ratio P_2/P_1 and the eccentricity, e_1 , in the GJ876 system with stochastic forcing corresponding to $D = 0.42\text{cm}^2/\text{s}^3$. The vertical lines indicate when the angles enter circulation for a prolonged period. The realisation illustrated in the lower panel scatters shortly after ϕ_1 goes into circulation.

6.2 Dependence on the Diffusion Coefficient

We now consider the stability of the systems listed in table 5.1 as a function of D . These systems have a variety of masses and orbital eccentricities. In particular, in view of the complex interaction between the resonant angles discussed above we wish to investigate whether the mean amplitude growth at a given time is indeed proportional to D . As also mentioned above, the value of the diffusion parameter D , that should be adopted, is very uncertain. We have therefore considered values of D ranging over five orders of magnitude. However, the correlation time τ_c is always taken to be given by $\tau_c = 0.5\Omega^{-1}$ while the RMS value of the force is changed. In order to determine the "lifetime" of a resonant angle, we monitor whether it is librating or circulating. Numerically, libration is defined to cease at the first time the angle is seen to reach absolute values larger than 2. We note that the angle can in general regain small values afterwards. However, this is a transient effect and changes the lifetime by no more than a factor of ~ 2 in all our simulations.

In this context we consider the fast angle ϕ_1 and the slow angle ζ , though, as we saw above, the latter can be replaced by ϕ_2 which exhibits the same behaviour. As ϕ_1 is the last to start circulating the resonance is defined to be broken at that point.

Equations (4.46) and (4.47) estimate the spreading of the resonant angles as a function of time. We determine the times to attain circulation as the times to attain $(\Delta\phi_i)^2 = 4, i = 1, 2$. We plot both the numerical and analytical results in figure 6.3. To remove statistical fluctuations and obtain a mean spreading time, the numerical values for a particular value of D were obtained by averaging over 60 realizations.

From figure 6.3 it is apparent that the evolutionary times scale is $\propto 1/D$ for D varying by many orders of magnitude. The analytic estimates for the libration survival times of ϕ_1 , dominated by the fast mode, obtained using equation (4.46) with the fast libration frequency determined from the simulations, are plotted in the upper panel of figure 6.3. These are in good agreement with the numerical results. However, the estimate for ϕ_2 based on equation (4.47) using the initial value of e_1 overestimates the lifetime by a factor of at least ~ 40 (see solid line in the lower plot of figure 6.3). Furthermore (4.47) has no dependence on planet mass which is in clear conflict with the numerical results. This, as discussed above is due to the temporary attainment of small eccentricities. This causes the disruption of the libration of ζ earlier than would be predicted assuming e_1 is constant. In fact this disruption occurs at times that can be up to a factor of 10 times shorter than those required to disrupt ϕ_1 . We estimate the lifetime of librations of ϕ_2 by calculating the time ϕ_1 needs to reach values close to 1 (see dashed lines in the lower plot of figure 6.3). As explained above in section 4.3.3, large amplitude variations of ϕ_1 are expected to couple to and excite the slow mode. Variations induced in the eccentricity e_1 allow this to reach zero and we lose libration of ϕ_2 . These simple estimates are in good agreement with the numerical results and accordingly support the idea that ϕ_1 and ϕ_2 are indeed coupled in the non linear regime. For low mass planets this simple analytic prediction underestimates the lifetime of ϕ_2 by a factor of ~ 2 , suggesting that the coupling between the two modes depends slightly on the planet masses.

To confirm our understanding of these processes, we have repeated the calculations with systems that are in the same state as the system discussed above but have higher eccentricities (see GJ876 LM HE and GJ876 SE HE in table 5.1). The lifetime of the librating state of ϕ_1 is unchanged, as this does not depend significantly on the eccentricity. However, the lifetime of the librating state of ϕ_2 is a factor of 2–3 longer. This is due to the fact that a larger excitation of ϕ_2 is needed to make e_1 reach small values in these simulations.

The random walk description breaks down completely when the anticipated disruption time

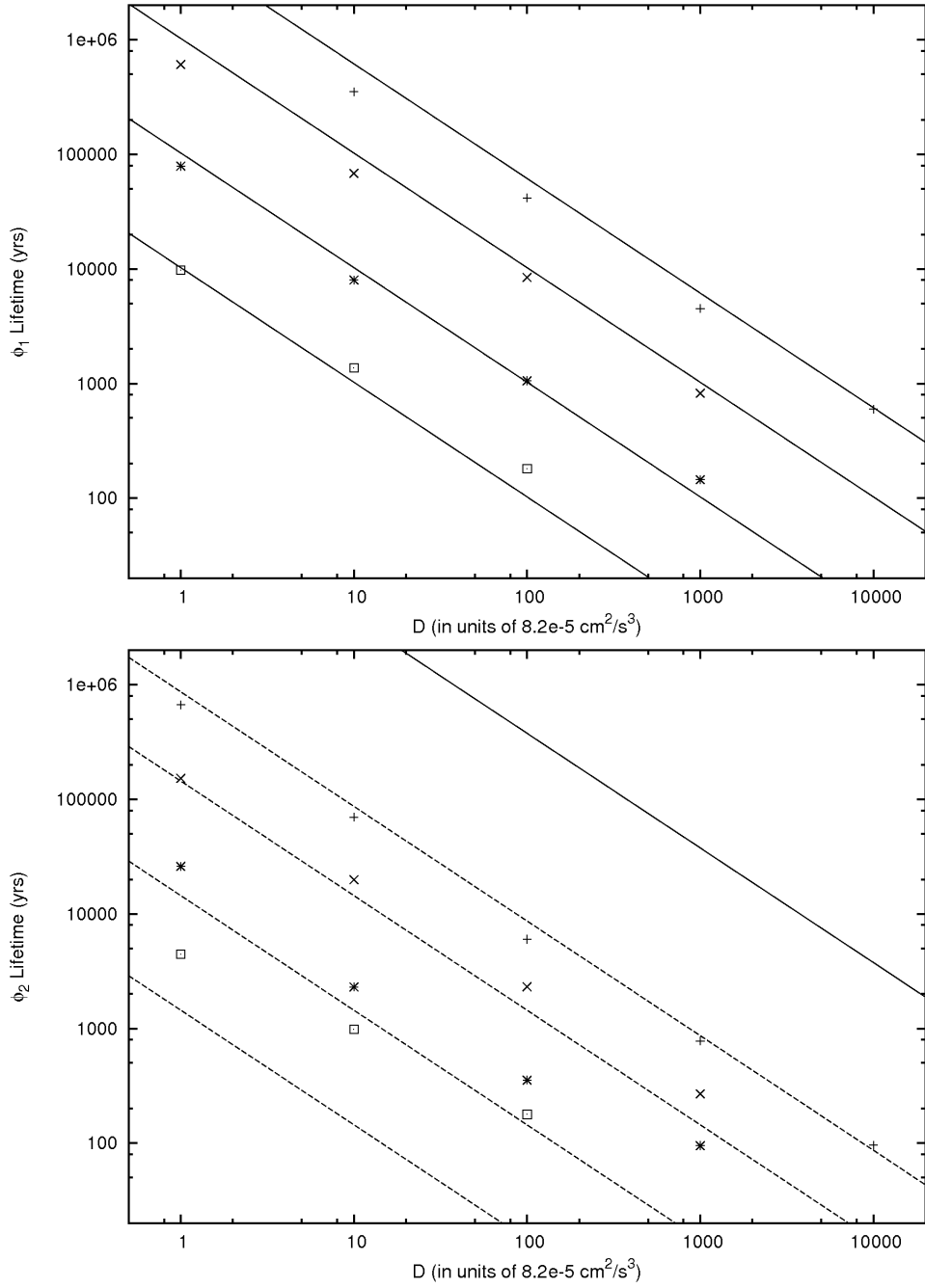


Figure 6.3: Average time until circulation of the resonant angles ϕ_1 (top) and ϕ_2 (bottom) in the GJ876 (indicated with +), GJ876LM (indicated with \times), GJ876SE (indicated with \star) and GJ876E (indicated with \square) systems as a function of the stochastic forcing diffusion coefficient D . In the case of the upper panel, the analytic curves explained in the text, are from top to bottom for the GJ876, GJ876LM, GJ876SE and GJ876E systems respectively. In the lower panel the analytic curves, as explained in the text, are from top to bottom for the GJ876 (solid curve and top dashed curve), GJ876LM, GJ876SE and GJ876E systems respectively.

becomes shorter than the libration period. This is expected to happen for small enough masses as can be verified from figure 6.3. It is because the disruption time decreases linearly with the planet masses while the libration period increases as the square root of the planet masses. Then we cannot average over many libration periods. This situation is apparent in figure 6.3 for very short disruption times of the order 100-1000 years where survival times cease to vary linearly with $1/D$.

Chapter 7

Formation of HD128311

We here discuss the application of the ideas discussed above to understanding the orbital configuration of the planetary system HD128311. This is (with 99% confidence) in a 2:1 mean motion resonance with the angle ϕ_1 librating and the angle ζ circulating so that there is no apsidal corotation (?). However, the orbital parameters are not well constrained. The original Keplerian fit by ? is such that the planets undergo a close encounter after only 2000 years. The values in table 5.1 have been obtained from a fit to the observational data that includes interactions between the planets. The values quoted have large error bars. For example the eccentricities e_1 and e_2 have an uncertainty of 33% and 21%, respectively. Although the best fit doesn't manifest apsidal corotation, the system could undergo large amplitude librations and still be stable.

According to ? the planets should have apsidal corotation if the commensurability was formed by the two planets undergoing sufficiently slow convergent inward migration, and if they then both migrated inwards significantly while maintaining the commensurability (see also ?). Accordingly ? suggested a possible formation scenario with inward migration as described above, but with an additional perturbing event, such as a close encounter with an additional planet occurring after the halting of the inward migration. This perturbation is needed to alter the behaviour of ζ , so that it undergoes circulation rather than libration and thus producing orbital parameters similar to the observed ones.

We showed above that stochastic forcing possibly resulting from turbulence driven by the MRI readily produces systems with commensurabilities without apsidal corotation if the eccentricities are not too large. This suggests that a scenario that forms the commensurability through disc induced inward convergent migration might readily produce commensurable systems without apsidal corotation if stochastic forcing is included. Such scenarios are investigated in this section.

We present simulations of the formation of HD128311 that include migration and stochastic forcing due to turbulence but do not invoke special perturbation events involving additional planets. We find that model systems with orbital parameters resembling the observed ones are readily produced that give better matches than so far provided by ?. The planets in this system are of the order of several Jupiter masses and the eccentricity of one planet can get very small during one libration period. The observed orbital parameters are plotted on the right hand side of figures 7.1, 7.2 and 7.3.

7.1 Migration Forces

We incorporate the non-conservative forces exerted by a protostellar disc that lead to inward migration by following the approach of ? and ?. In this the migration process is characterized by migration and eccentricity damping timescales, $\tau_a = a/\dot{a}$ and $\tau_e = e/\dot{e}$. We also define the ratio of the above timescales to be $K = |\tau_a|/\tau_e$. This ratio determines the eccentricities in the state of self similar inward migration of the commensurable system that is attained after large times. We verify this result for two different values of K (see below). The procedure is now widely used (e.g. ??) and we have checked our code against the results of their work.

In this work we allow the planets to form a commensurability through convergent inward migration but stochastic forcing is included, the disc is then removed through having its surface density reduced to zero on a prescribed timescale. This simultaneously reduces both the migration forces and the stochastic forcing to zero. This procedure is very similar to that adopted by the above authors but we have included stochastic forcing and removed the disc on longer time scales.

The stochastic forces have to have the right balance with respect to the migration rate. We have found that inward migration imparts stability to the resonant system. If the migration rate is too fast relative to the stochastic forcing the migration keeps down the libration amplitudes and we do not get circulation. On the other hand large eccentricity damping favours broken apsidal corotation. This might look counterintuitive at first sight, but remember that the diffusion of ζ depends on $1/e_{1,2}^2$. Due to the stochastic nature of the problem, it is hard to present a continuum of solutions so we restrict ourselves to the discussion of three representative examples. However, we comment that we are able to obtain similar end states for a wide range of migration parameters. Before presenting these examples we briefly indicate how the librations can be stabilized by the migration process.

As above, the parameters $\langle F_i \rangle$ and τ_c are kept constant, so maintaining D constant, for the duration of the simulation, with τ_c being determined for the initial location of the outer planet. As discussed above, these values may scale with the radius of the planet and we thus expect them to change during migration. However, the semi major axis of the outer planet changes only by $\sim 30\%$ during the simulation consequently we ignore this effect.

7.2 Adiabatic Invariance and the Stabilization of Librations through Migration

Both the fast angle ϕ_1 and the slow angle ϕ_2 obey stochastically forced oscillator equations (4.33). Although we do not have a simple expressions for the oscillation frequencies we know that for fixed eccentricity and planet masses they both scale as the orbital frequency, n_1 . When the planets migrate inwards together, this increases slowly with time. Accordingly the theory of adiabatic invariance indicates that the libration amplitude should scale as $n_1^{-1/2}$. If there were no stochastic forcing this would decrease on twice the migration time scale $2\tau_a$. Suppose the time to attain a root mean square amplitude of unity in the absence of migration is τ_{stoch} , we would then expect the migration to be able to control the libration if τ_a is significantly less than τ_{stoch} . Note that the angle ϕ_2 remains vulnerable to large changes if eccentricities become small and statistical arguments would suggest eventual disruption but on a significantly increased timescale in the case of ϕ_1 .

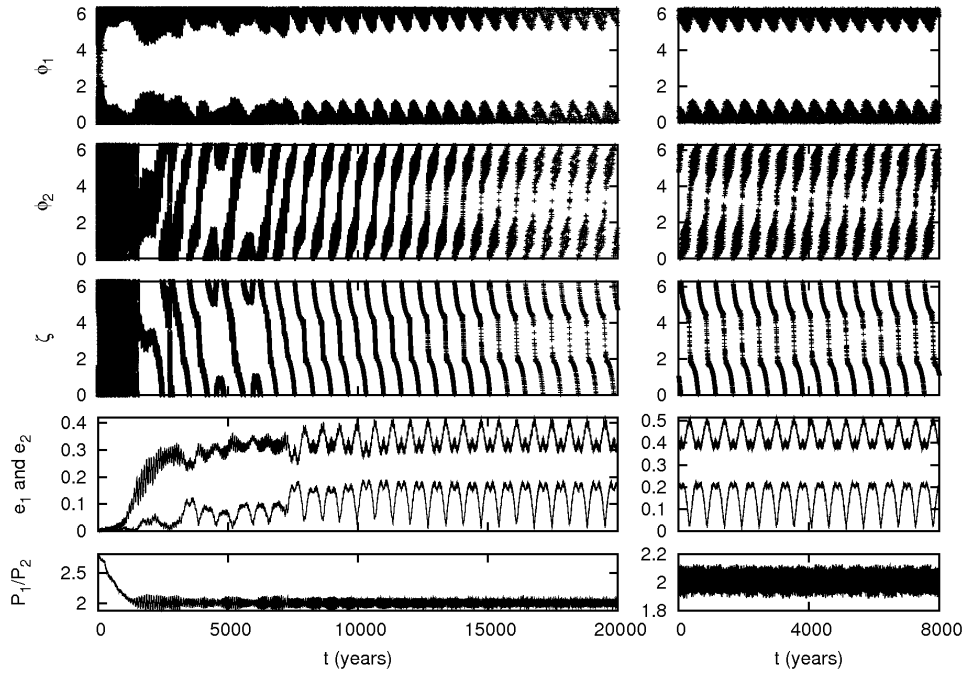


Figure 7.1: The plots on the left hand side show a possible formation scenario of HD128311. We plot the observed system on the right hand side as a comparison (see table 5.1 and text). The plots show the resonant angles ϕ_1, ϕ_2, ζ , the eccentricities e_1, e_2 and period ratio P_1/P_2 for formation scenarios including turbulence and migration. Resonance capturing occurs after 2000 years. The stochastic forces make ϕ_2 and ζ circulate while ϕ_1 is in libration. After the disc forces are slowly removed, the system is in a stable configuration that is extremely similar to the observed system. The damping parameters in this run are $\tau_{a,1} = 8000$, $\tau_{a,2} = -20000$ and $K = 8$.

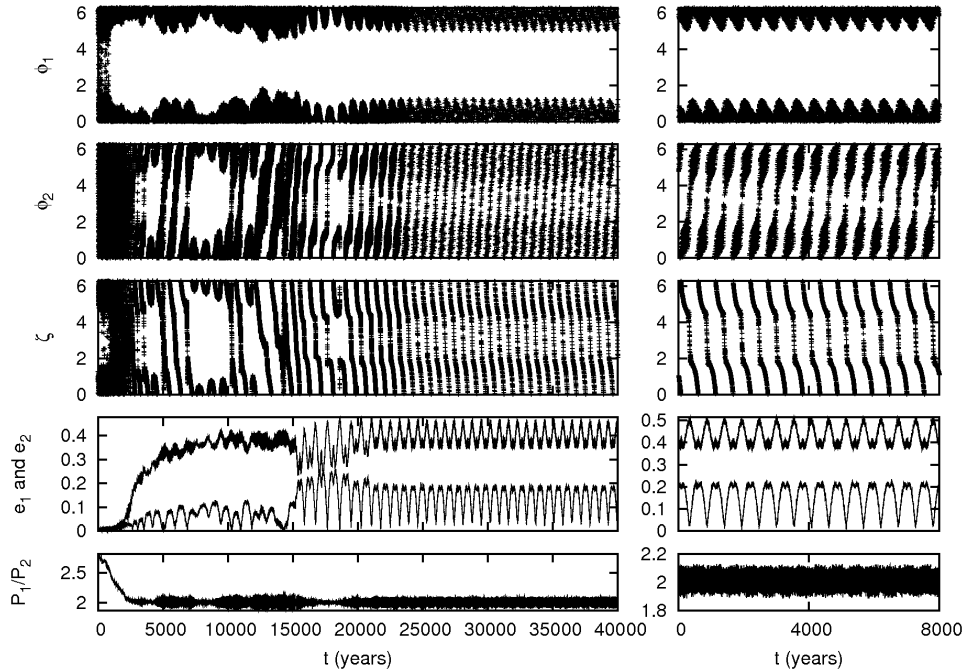


Figure 7.2: The plots on the left hand side show another possible formation scenario of HD128311. Again, we plot the observed system on the right hand side as a comparison (see table 5.1 and text). The migration timescales in this run are $\tau_{a,1} = 16000$, $\tau_{a,2} = -40000$ and $K = 5.5$. Note that the eccentricities are larger compared to figure 7.1 because K is smaller.

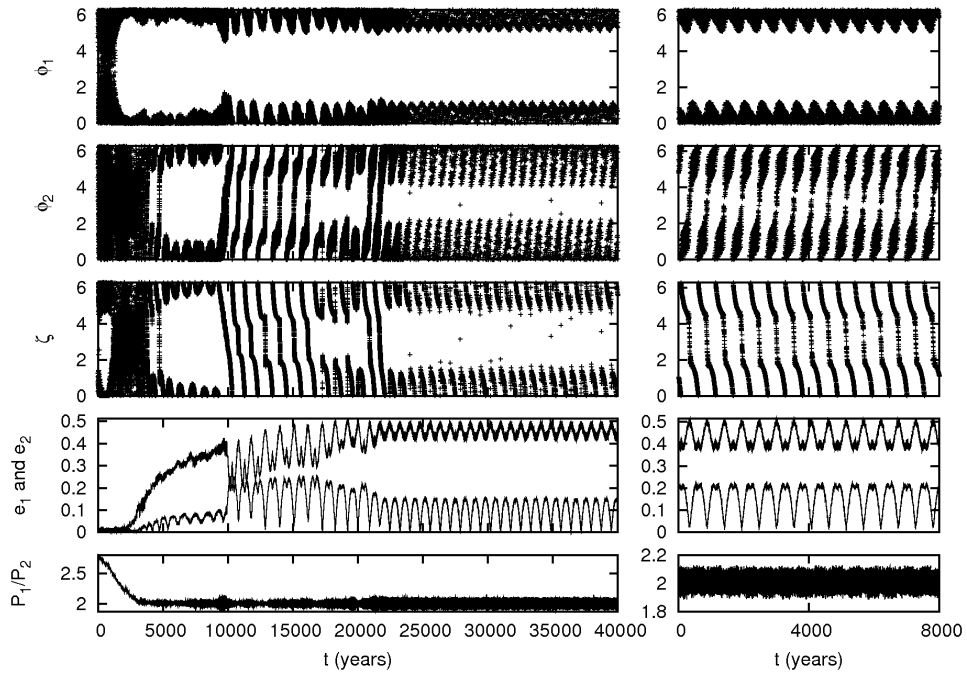


Figure 7.3: These plots show another possible formation scenario of HD128311. The damping parameters are the same as in figure 7.2. It is not clear whether the final state possesses apsidal corotation or not.

7.3 Model 1

The planets are initially in circular orbits at radii $a_1 = 4$ AU and $a_2 = 2$ AU. Stochastic forcing is applied to the outer planet only with the diffusion coefficient $D = 6.4 \cdot 10^{-3} \text{cm}^2/\text{s}^3$. Note that although this value is 640 times larger than the scaling given by equation (5.3), corresponding to a force that is 25 times larger than the simple estimate given in section 5.1, corresponding to smaller reduction factors resulting from a gap or dead zone, it is too small for the angle ϕ_1 to be brought to circulation during our runs. The results given above and summarized in figure 6.3, and other tests, indicate that similar results would be obtained if D is reduced, but on a longer time scale $\propto 1/D$, provided the migration rate is also appropriately ultimately reduced so that the system can survive for long enough to enable ζ to be driven into circulation.

The outer planet is made to migrate inwards on a timescale $\tau_{a_1} = 8000$ years. The inner planet migrated slowly outwards on a timescale of $\tau_{a,2} = -20000$ years. This results in convergent migration. For both planets we use an eccentricity to semi major axis damping ratio of $K = 8$. The resulting evolutionary timescales are significantly larger than those used by eg. ? and more easily justified by hydrodynamical simulations.

The time evolution is shown in the left plot of figure 7.1. After resonance capturing all angles are either initially librating or on the border between libration and circulation. The slow mode has a period of ~ 700 years, whereas the slow mode period is 20 times shorter.

It can be seen from figure 7.1 and other related figures below, that while migration continues libration amplitudes tend to be controlled apart from when e_1 becomes either zero or very close to zero. Then, due to stochastic forcing, ϕ_2 and ζ start circulating. Subsequently libration is recovered over time intervals for which e_1 does not attain very small values but eventually additional stochastic forcing together with the repeated attainment of small values for e_1 causes ϕ_2 to remain circulating for the remainder of the simulation. After 13000 years, both the forces due to migration and turbulence are reduced smoothly on a timescale of 2000 years. The result is a stable configuration that resembles the observed system very well.

7.4 Model 2

For this simulation, we lengthened the migration timescales by a factor of 2 to show that the results are generic. We also decreased the value of K to 5.5. This results in larger eccentricities and the final state better resembled our representation of the observed system. However, it should be kept in mind that the eccentricities are not well constrained by the observations. All other parameters are the same as for model 1. The time evolution is plotted in figure 7.2. The resonant angles librate immediately after the capture into resonance as predicted for sufficiently slow migration. However, in the same way as for model 1 described above, stochastic forces make ϕ_2 circulate soon afterwards. Once the migration forces and stochastic forces are removed between 20000 and 22000 years, the system stays in a stable configuration with no apsidal corotation.

7.5 Model 3

All parameters are the same as for model 2. Accordingly model 3 represents another statistical realization of that case. The time evolution is plotted in figure 7.3. The final state is very close to the boundary between libration and circulation of ζ . As discussed above, large uncertainties in the orbital parameters means that the actual system could be in such a state.

Due to stochastic forces, which may result from local turbulence, we are able to generate a broad spectrum of model systems. Some of them undergo a strong scattering during the migration process. However, the surviving systems resemble the observed system very well. Although the orbital parameters are not well constrained yet, we showed that values in the right range are naturally produced by a turbulent disc.

Chapter 8

Discussion

In this essay, we have presented a self consistent analytic model applicable to either a single planet or two planets in a mean motion resonance subject to external stochastic forcing. The stochastic forces could result from MRI driven turbulence within the protoplanetary disc but our treatment is equally applicable to any other source.

We considered the evolution of a stochastically forced two planet system that is initially deep inside a MMR (ie. the two independent resonant angles librate with small amplitude). Stochastic forces cause libration amplitudes to increase in the mean with time until all resonant angles are driven into circulation at which point the commensurability is lost. Often a strong scattering occurs soon afterwards for systems composed of planets in the Jovian mass range.

We isolated a fast libration mode which is associated with oscillations of the semi-major axes and a slow libration mode which is mostly associated with the motion of the angle between the apsidal lines of the two planets. These modes respond differently to stochastic forcing, the slow mode being more readily converted to circulation than the fast mode. This slow mode is sensitive to the attainment of small eccentricities which cause rapid transitions between libration and circulation. The amplitude of the fast mode grows more regularly in the mean, with the square of the libration amplitude in most cases increasing linearly with time and being proportional to the diffusion coefficient D . Of course this discussion is simplified and there are limitations. For example if the total mass of the system is reduced, the disruption time eventually becomes comparable to the libration period. In that case the averaging process that we used in the derivation is no longer valid and the lifetime no longer scales as $1/D$.

The analytic model was compared with numerical simulations which incorporated stochastic forces. Those forces, parameterized by the mean square values of each component in cylindrical coordinates and the autocorrelation time, were applied in a continuous manner giving results that could be directly compared with the analytic model. The simulations were in broad agreement with analytic predictions and we presented illustrative examples of the disruption process. We performed the simulations for a large range of diffusion parameters, planet masses and initial eccentricities to verify the scaling law for the commensurability disruption time summarized hereafter.

To summarize our results, recalling that the slow angle is driven into circulation before the fast angle, so that the ultimate lifetime is determined by the time taken for the fast angle to achieve circulation, we determine the lifetime, t_f , using equation (4.46) setting $t = t_f$, $(\Delta Q)^2 = (\Delta Q)_0^2 = 4$, together with $\gamma_f = p = 1$, so obtaining

$$t_f = \frac{a_1^2 \omega_{l_f}^2 (\Delta Q)_0^2}{36D}. \quad (8.1)$$

We showed above that this gives good agreement with our numerical results. Using $D = 2\langle F_i^2 \rangle \tau_c$, we can express this result in terms of the relative magnitude of the stochastic forcing in the form

$$t_f = 2.4 \times 10^{-4} \left(\frac{a_1^2 n_1^4}{\langle F_i^2 \rangle} \right) \left(\frac{(\Delta Q)_0^2}{8n_1 \tau_c} \right) \left(\frac{8.5 \omega_{lf} \sqrt{q_{GJ}}}{n_1 \sqrt{q}} \right)^2 \frac{q}{q_{GJ}} P_1, \quad (8.2)$$

where P_1 is the orbital period of the outer planet. Here the first quantity in brackets represents the ratio of the square of the central force per unit mass to the mean square stochastic force per unit mass acting on the outer planet. The other quantities in brackets, scaled to the GJ876 system are expected to be unity, while the last factor q/q_{GJ} is the ratio of the total mass ratio of the system to the same quantity for GJ876. Here it is assumed that the two planets in the system have comparable masses.

From (8.2) we see that a non migrating system such as GJ876 could survive in resonance for $t_f \sim 10^6$ years if the stochastic force amplitude is $\sim 10^{-5}$ times the central force. This expression enables scaling to other systems at other disc locations for other stochastic forcing amplitudes. Inference of survival probabilities for particular systems depends on many uncertain aspects, such as the protoplanetary disc model and the strength of MRI turbulence. However, the mass ratio dependence in equation (8.2) indicates that survival is favored for more massive systems. At the present time the number of observed resonant systems is too small for definitive conclusions to be made. However, the fact that several systems exhibiting commensurabilities have been observed indicates that resonances are not always completely disrupted by stochastic forces due to turbulence, but rather may be modified as in our study of HD128311.

The HD128311 system is such that the fast mode librates with the slow mode being near the borderline between libration and circulation. We found that such a configuration was readily produced in a scenario in which the commensurability was formed through a temporary period of convergent migration with the addition of stochastic forcing. During a migration phase moderate adiabatic invariance applied to the libration modes together with eccentricity damping leads to increased stabilization and a longer lifetime for the resonance. However, as discussed above, the time evolution of the eccentricity and in particular the attainment of small values plays an important role in causing the slow mode to circulate corresponding to the loss of apsidal corotation. Thus we expect that a large eccentricity damping rate does not necessarily stabilize the apsidal corotation of the system. Additional simulations have shown that this resonance is lost more easily for large damping rates ($K \gg 10$).

Further observations of extrasolar planetary systems leading to better statistics may lead to an improved situation for assessing the role of stochastic forcing with the model presented above in future. We will then be able to determine both the strength and the duration of turbulence in protoplanetary discs from observations of multiple planetary systems only. A better understanding of the astrophysical processes during planet formation will also lead to a better understanding of our own solar system and eventually Earth.

Chapter 9

Acknowledgements

I would like to thank John Papaloizou for his support throughout this work. I am also indebted to Sijme-Jan Paardekooper for keeping the Hyades cluster running. Financial support was provided by an Isaac Newton studentship, an STFC studentship, St John's College and the Department of Applied Mathematics and Theoretical Physics.

Part III
Appendix

Appendix A

Units and Symbols

In this chapter, I define units, constants and symbols that I used within this essay. Note that several symbols have multiple meanings, depending on the context.

Unit / Constant	Value
Length	
1 AU (Astronomical Unit)	$1.49598 \cdot 10^8$ km $1.49598 \cdot 10^{13}$ cm
1 pc (Parsec)	$3.0857 \cdot 10^{13}$ km
Mass	
1 M_{\odot} (Solar Mass)	$1.9891 \cdot 10^{30}$ kg
1 M_{Jup} (Jupiter Mass)	$1.8986 \cdot 10^{27}$ kg $0.9545 \cdot 10^{-3} M_{\odot}$
1 M_{Earth} (Earth Mass)	$5.9736 \cdot 10^{24}$ kg $3.0032 \cdot 10^{-6} M_{\odot}$
Time	
1 year	$3.156 \cdot 10^7$ s
Gravitational Constant	
G	$6.674 \cdot 10^{-8}$ $\text{cm}^3\text{g}^{-1}\text{s}^{-2}$
GM_{\odot}	39.49 $\text{AU}^3\text{year}^{-2}$

Symbol	Definition / Name
$T = 2\pi/\Omega$	Orbital Period
Ω	Orbital Frequency
m	Mass of the Planet
M	Mass of the Star
a	Semi-Major Axis
b	Semi-Minor Axis
e	Eccentricity
ϖ	Longitude of Pericentre
Ω	Longitude of Ascending Node
i	Inclination
M	Mean Anomaly
E	Eccentric Anomaly
θ	True Longitude
λ	Mean Longitude
n	Mean Motion
\vec{n}	Ascending Node
ϕ_1, ϕ_2	Resonant Angles
ζ	"Slow Mode" in Resonant Angles
Q	"Fast Mode" in Resonant Angles
$\Delta\varpi$	Difference of Apssidal Lines (Two Planets)
H	Hamultonian
E	Energy
L	Angular Momentum
F	Force
Δt	Timestep
τ_a	Migration Timescale
τ_e	Eccentricity Damping Timescale
K	Ratio of τ_a/τ_e
τ_c	Correlation Time of Turbulent Forces
$g(t)$	Autocorrelation Function of Turbulent Forces
Σ	Surface Density of the Protostellar Disc
D	Random Walk Diffusion Parameter
$C_{k,l}, D_{k,l}, E_{k,l}, F_{k,l}$	Coefficients in Expansion of Hamiltonian
$\gamma, \gamma_f, \gamma_s$	Reduction Factors

Appendix B

Dissipative Forces on Planets

We show how the additional terms due to eccentricity and semi-major axis damping are derived. The procedure follows ? and some expressions are taken from ?.

We have additional terms for both, velocity and acceleration. In a Cartesian coordinate system, we get

$$\left. \frac{dx}{dt} \right|_{\dot{a}} + \left. \frac{dx}{dt} \right|_{\dot{e}} = \frac{\partial x}{\partial a} \dot{a} + \frac{\partial x}{\partial e} \dot{e}, \quad (\text{B.1})$$

$$\left. \frac{d\dot{x}}{dt} \right|_{\dot{a}} + \left. \frac{d\dot{x}}{dt} \right|_{\dot{e}} = \frac{\partial \dot{x}}{\partial a} \dot{a} + \frac{\partial \dot{x}}{\partial e} \dot{e}. \quad (\text{B.2})$$

The expressions are similar for the other coordinates. In order to differentiate with respect to a and e , we have to write these expressions in terms of orbital elements

$$\begin{aligned} x &= r \cos \Omega \cos (\omega + f) - r \cos i \sin \Omega \sin (\omega + f), \\ y &= r \sin \Omega \cos (\omega + f) + r \cos i \cos \Omega \sin (\omega + f), \\ z &= r \sin i \sin (\omega + f). \end{aligned} \quad (\text{B.3})$$

This follows from the definition of the orbital parameters. See figure 2.1 in the chapter about orbital parameters. By differentiating once, we get

$$\begin{aligned} \dot{x} &= \cos \Omega [\dot{r} \cos (\omega + f) - r \dot{f} \sin (\omega + f)] \\ &\quad - \cos i \sin \Omega [\dot{r} \sin (\omega + f) + r \dot{f} \cos (\omega + f)], \\ \dot{y} &= \sin \Omega [\dot{r} \cos (\omega + f) - r \dot{f} \sin (\omega + f)] \\ &\quad + \cos i \cos \Omega [\dot{r} \sin (\omega + f) + r \dot{f} \cos (\omega + f)], \\ \dot{z} &= \sin i [\dot{r} \sin (\omega + f) + r \dot{f} \cos (\omega + f)]. \end{aligned} \quad (\text{B.4})$$

We also need r , \dot{r} , and $r \dot{f}$ in terms of a , e , and f :

$$r = \frac{a(1 - e^2)}{1 + e \cos f} \quad (\text{B.5})$$

$$\dot{r} = \frac{r \dot{f} e \sin f}{1 + e \cos f} \quad (\text{B.6})$$

$$r \dot{f} = \frac{na}{\sqrt{1 - e^2}} (1 + e \cos f). \quad (\text{B.7})$$

To complete the list of equations, we compute several other derivatives needed to calculate the partial derivatives in equation (B.1) and (B.2)

$$\begin{aligned}
\frac{\partial r}{\partial a} &= \frac{r}{a}, \\
\frac{\partial r}{\partial e} &= \left[-\frac{2er}{1-e^2} - \frac{r^2 \cos f}{a(1-e^2)} \right], \\
\frac{\partial \dot{r}}{\partial a} &= -\frac{\dot{r}}{2a}, \\
\frac{\partial \dot{r}}{\partial e} &= \frac{\dot{r}}{e(1-e^2)}, \\
\frac{\partial(r\dot{f})}{\partial a} &= -\frac{r\dot{f}}{2a}, \\
\frac{\partial(r\dot{f})}{\partial e} &= \frac{r\dot{f}(e + \cos f)}{(1-e^2)(1+e \cos f)}.
\end{aligned} \tag{B.8}$$

Putting everything together, we arrive at new expressions

$$\left. \frac{dx}{dt} \right|_{\dot{a}} + \left. \frac{dx}{dt} \right|_{\dot{e}} = \frac{x}{a} \dot{a} + \left[\frac{r}{a(1-e^2)} - \frac{1+e^2}{1-e^2} \right] \frac{x}{e} \dot{e}, \tag{B.9}$$

$$\left. \frac{dy}{dt} \right|_{\dot{a}} + \left. \frac{dy}{dt} \right|_{\dot{e}} = \frac{y}{a} \dot{a} + \left[\frac{r}{a(1-e^2)} - \frac{1+e^2}{1-e^2} \right] \frac{y}{e} \dot{e}, \tag{B.10}$$

$$\left. \frac{dz}{dt} \right|_{\dot{a}} + \left. \frac{dz}{dt} \right|_{\dot{e}} = \frac{z}{a} \dot{a} + \left[\frac{r}{a(1-e^2)} - \frac{1+e^2}{1-e^2} \right] \frac{z}{e} \dot{e}. \tag{B.11}$$

The additional terms for each of \dot{x}/dt , \dot{y}/dt , \dot{z}/dt are distinct for variations in e :

$$\begin{aligned}
\left. \frac{d\dot{x}}{dt} \right|_{\dot{a}} + \left. \frac{d\dot{x}}{dt} \right|_{\dot{e}} &= -\frac{\dot{x}}{2a} \dot{a} + \cos \Omega \left[\frac{\partial \dot{r}}{\partial e} \cos(\omega + f) - \frac{\partial(r\dot{f})}{\partial e} \sin(\omega + f) \right] \dot{e} \\
&\quad - \cos i \sin \Omega \left[\frac{\partial \dot{r}}{\partial e} \sin(\omega + f) + \frac{\partial(r\dot{f})}{\partial e} \cos(\omega + f) \right] \dot{e},
\end{aligned} \tag{B.12}$$

$$\begin{aligned}
\left. \frac{d\dot{y}}{dt} \right|_{\dot{a}} + \left. \frac{d\dot{y}}{dt} \right|_{\dot{e}} &= -\frac{\dot{y}}{2a} \dot{a} + \sin \Omega \left[\frac{\partial \dot{r}}{\partial e} \cos(\omega + f) - \frac{\partial(r\dot{f})}{\partial e} \sin(\omega + f) \right] \dot{e} \\
&\quad + \cos i \cos \Omega \left[\frac{\partial \dot{r}}{\partial e} \sin(\omega + f) + \frac{\partial(r\dot{f})}{\partial e} \cos(\omega + f) \right] \dot{e},
\end{aligned} \tag{B.13}$$

$$\left. \frac{d\dot{z}}{dt} \right|_{\dot{a}} + \left. \frac{d\dot{z}}{dt} \right|_{\dot{e}} = -\frac{\dot{z}}{2a} \dot{a} + \sin i \left[\frac{\partial \dot{r}}{\partial e} \sin(\omega + f) + \frac{\partial(r\dot{f})}{\partial e} \cos(\omega + f) \right] \dot{e}. \tag{B.14}$$

The final equations (B.9-B.14) are used to calculate the terms due to the dissipative forces and included in my N-body code (see section 2.1). Note that we have to calculate the orbital elements every (sub-)timestep.

Appendix C

Calculating Orbital Elements

In this chapter we present the method we used for calculating orbital elements from given position and velocity vectors, \mathbf{x} , \mathbf{v} . Although the definition of orbital elements is straightforward (see section 2.4), the actual calculation is more complicated, as several numbers can be very small and rounding errors can lead to floating point exceptions.

In a system with multiple planets, we first calculate the orbit of the innermost planet. Then the centre of mass (of this planet and the star) is calculated and used as an origin for the orbit of the second planet. This process is iterated if required.

We work in units where $G = 1$ and the mass is measured in solar masses M_\odot . Vector components have subscripts 0, 1, 2 (C-style) and magnitudes of vectors have no index.

First of all, we calculate the specific angular momentum vector and its magnitude:

$$\mathbf{h} = \mathbf{r} \times \mathbf{v} \quad (\text{C.1})$$

$$h = \sqrt{h_0^2 + h_1^2 + h_2^2}. \quad (\text{C.2})$$

We also calculate the normalized dot product between \mathbf{v} and \mathbf{r}

$$vr \equiv (r_0v_0 + r_1v_1 + r_2v_2)/r. \quad (\text{C.3})$$

By using the standard gravitational parameter $\mu = M_* + m$, which is the sum of the star and planet mass, we can calculate the eccentricity vector

$$e_0 = \frac{1}{\mu} ((v^2 - \mu/r) \cdot r_0 - r \cdot vr \cdot v_0) \quad (\text{C.4})$$

$$e_1 = \frac{1}{\mu} ((v^2 - \mu/r) \cdot r_1 - r \cdot vr \cdot v_1) \quad (\text{C.5})$$

$$e_2 = \frac{1}{\mu} ((v^2 - \mu/r) \cdot r_2 - r \cdot vr \cdot v_2). \quad (\text{C.6})$$

Its amplitude is the eccentricity. The semi-major axis, and therefore by (1.1) the orbital period is given by

$$a = -\mu / (v^2 - 2 \cdot \mu/r) \quad (\text{C.7})$$

$$P = 2\pi \sqrt{a^3/\mu}. \quad (\text{C.8})$$

The inclination is given by the angle of the angular momentum vector relative to the xy -plane

$$i = \arccos(h_2/h). \quad (\text{C.9})$$

If $\pi/2 < i < \pi$ then, the orbit is retrograde in our coordinate system (per definition). The vector of nodes \mathbf{n} lies in the xy -plane (again, per definition) the x and y components are

$$n_0 = -h_1 \quad \text{and} \quad n_1 = h_0. \quad (\text{C.10})$$

If the orbit is exactly in the xy -plane, or very close to it, the node line is not defined. Numerically, we check if either i or n (absolute value of the node vector, not the mean motion) is less than $1 \cdot 10^{-30}$. In that case, we set the longitude of the ascending node Ω equal to 0 and calculate the longitude of pericentre (with respect to the Cartesian x -axis) as follows

$$\bar{\omega} = \begin{cases} \arccos(e_0/e) & \text{if } e_1 \geq 0 \\ 2\pi - \arccos(e_0/e) & \text{if } e_1 < 0. \end{cases} \quad (\text{C.11})$$

If the orbit is not in the xy -plane, we calculate the longitude of pericentre (with respect to the ascending node)

$$\bar{\omega} = \begin{cases} \arccos[(n_0 \cdot e_0 + n_1 \cdot e_1) / (n \cdot e)] & \text{if } e_2 \geq 0 \\ 2\pi - \arccos[(n_0 \cdot e_0 + n_1 \cdot e_1) / (n \cdot e)] & \text{if } e_2 < 0. \end{cases} \quad (\text{C.12})$$

The longitude of the ascending node (with respect the the x -axis) is

$$\Omega = \begin{cases} \arccos(n_0/n) & \text{if } n_1 \geq 0 \\ 2\pi - \arccos(n_0/n) & \text{if } n_1 < 0. \end{cases} \quad (\text{C.13})$$

After each call of $\arccos()$ we have to check if a rounding error occurred and if the returned value is NaN or INF. The true and eccentric anomalies are given by

$$f = \begin{cases} \arccos[\mathbf{e} \cdot \mathbf{r} / (e \cdot r)] & \text{if } vr \geq 0 \\ 2\pi - \arccos[\mathbf{e} \cdot \mathbf{r} / (e \cdot r)] & \text{if } vr < 0, \end{cases} \quad (\text{C.14})$$

$$E = \begin{cases} \arccos[(1 - r/a) / e] & \text{if } vr \geq 0 \\ 2\pi - \arccos[(1 - r/a) / e] & \text{if } vr < 0. \end{cases} \quad (\text{C.15})$$

Finally, we calculate the mean longitude

$$\lambda = E - e \sin E + \bar{\omega}. \quad (\text{C.16})$$

If we are in a circular orbit, $\bar{\omega}, f, \lambda$ have no meaning. We set them equal to zero, if $e \leq 10^{-10}$.